Human-in-the-Loop Optimization of Exoskeleton Assistance Via Online Simulation of Metabolic Cost

Daniel F. N. Gordon, Christopher McGreavy, Andreas Christou, and Sethu Vijayakumar

***Abstract*—Many assistive robotic devices have been developed to augment or assist human locomotion. Despite advancements in design and control algorithms, this task remains challenging. Human walking strategies are unique and complex, and assistance strategies based on the dynamics of unassisted locomotion typically offer only modest reductions to the metabolic cost of walking. Recently, human-in-the-loop (HIL) methodologies have been used to identify subject-specific assistive strategies, which offer significant improvements to energy savings. However, current implementations suffer from long measurement times, necessitating the use of low-dimensional control parameterizations, and possibly requiring multiday collection protocols to avoid subject fatigue. We present a HIL methodology, which optimizes the assistive torques provided by a powered hip exoskeleton. Using musculoskeletal modeling, we are able to evaluate simulated metabolic rate online. We applied our methodology to identify assistive torque profiles for seven subjects walking on a treadmill, and found greater reductions to metabolic cost when compared to generic or off-the-shelf controllers. In a secondary investigation, we directly compare simulated and measured metabolic rate for three subjects experiencing a range of assistance levels. The time investment required to identify assistance strategies via our protocol is significantly lower when compared to existing protocols relying on calorimetry. In the future, frameworks such as these could be used to enable shorter HIL protocols or exploit more complex control parameterizations for greater energy savings.**

***Index Terms*—Assistive robotics, exoskeletons, human-in-the-loop optimization, musculoskeletal modeling.**

I. Introduction

FOR decades, assistive robotic devices such as exoskeletons, exosuits, and prosthetic limbs have been a topic of major interest in the biomechanics and robotics communities [1]. Many of these developed platforms [2] are thought to have huge potential in a wide range of application domains related to human movement. For example, devices such as the Lokomat [3], a gait rehabilitation robot, have demonstrated the potential to be more effective than conventional treatments at restoring mobility to patients with spinal cord injuries [4]. Passive exoskeletons are being developed to help reduce the potential for strain-related injuries in the work-place [5], or to reduce the energy required for locomotion [6]. New powered ankle prostheses continue to be designed with the goal of replicating the energy efficiency of the biological human ankle [7], [8].

A particularly common design goal for powered exoskeletons and exosuits is to reduce the metabolic cost of walking [9]–[12]. Devices, which achieve this goal could be used either to augment human locomotion capabilities, for example to assist humans carrying heavy loads over long distances [13], or for long-term mobility rehabilitation or assistance of movement-impaired or elderly people [14]. This latter use case is of particular relevance to modern society, which increasingly faces the issue of mobility loss tied to an aging population [15], [16] along with the associated health problems and reduction in quality of life [17]. However, designing exoskeleton controllers, which can efficiently assist human locomotion has proven to be a challenging problem, as the efficacy of these devices is strongly dependent on the timing and magnitude of the delivered assistance [18]–[22]. Moreover, this issue is compounded by the fact that, due to variations in age, size, limb proportions, and even internal locomotion strategies, humans can exhibit significant differences in walking styles [23]–[25]. The consequence of this is that generic exoskeleton controllers may be suboptimal for a large number of individuals.

Recently, a solution to this problem has emerged in the form of human-in-the-loop (HIL) optimization. HIL optimization (see Fig. 1) is a technique, which seeks to optimize some aspect of an assistive device by iteratively taking measurements from the intended wearer "in the loop," evaluating device performance according to some metric and updating the system accordingly. Ultimately, the aim of this process is to produce a tailored assistance solution for each individual. Typically this process is used to optimize a parameterised control law [26]–[28], though other objectives have included step frequency [29], [30], parameterised design variables [31], and the energetic profile of assisted locomotion [32]. Most commonly, device performance is evaluated by quantifying metabolic rate via respiratory gas analysis [26]–[30], however, other physiological signals such as EMG activity [31], [33], or subject feedback [34], [35] have successfully been used as a performance criterion. A critical

Manuscript received June 30, 2021; revised October 29, 2021; accepted November 17, 2021. This work was supported in part by the EPSRC through the Centre for Doctoral Training in Robotics and Autonomous Systems under Grant EP/L016834/1, in part by the European Commission through the H2020 project Memory of Motion under Grant MEMMO, 780684, in part by the Alan Turing Institute, U.K., and in part by the Honda Research Institute Europe, Germany. This paper was recommended for publication by Associate Editor Lynch, Kevin and Editor M. Yim upon evaluation of the reviewers' comments. *(Corresponding author: Daniel F. N. Gordon.)*

Daniel F. N. Gordon and Sethu Vijayakumar are with the School of Informatics, The University of Edinburgh, Edinburgh EH89AB, U.K., and also with the Alan Turing Institute, London NW12DB, U.K. (e-mail: daniel.gordon@ed.ac.uk; sethu.vijayakumar@ed.ac.uk).

Christopher McGreavy and Andreas Christou are with the School of Informatics, The University of Edinburgh, Edinburgh EH89AB, U.K. (e-mail: ca.mcgreavy@gmail.com; andreas.christou@ed.ac.uk).

Color versions of one or more figures in this article are available at https://doi.org/10.1109/TRO.2021.3133137.

Digital Object Identifier 10.1109/TRO.2021.3133137

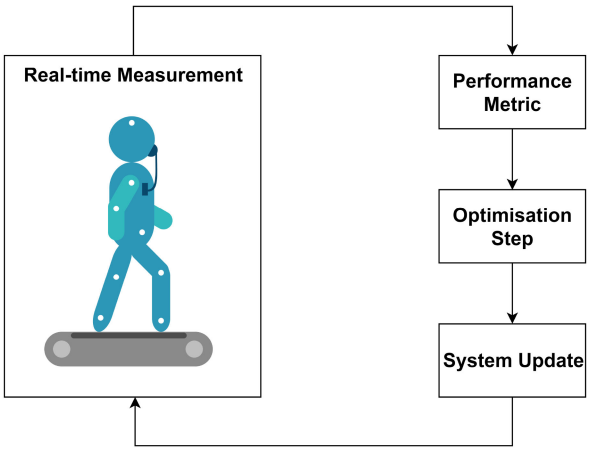

Fig. 1. Schematic illustrating the key steps comprising a generic implementation of HIL optimization. To illustrate, a specific implementation [28] could use calorimetry (the real-time measurement) to quantify metabolic cost (the performance metric) while using Bayesian optimization (the optimization step) to update some parameterised control law (the system update).

aspect of HIL optimization is the technique used to drive the update of system parameters, which must be efficient in order to promote convergence [30]. Two widely used and successful methods are covariance matrix adaptation [27] and Bayesian optimization [28], [30], which have comparable performance [32]. Other implementations have utilised reinforcement learning frameworks to optimize exoskeleton [33], [36] and prosthesis [37]–[39] control parameters. In general, using HIL optimization, researchers have been able to identify individualized control patterns, which result in significantly greater energetic savings than traditional control schemes [28].

Despite the impressive energetic cost reductions achieved by existing HIL optimization implementations, a clear limitation of the method exists: the significant time investment required to produce optimized assistance profiles. This is particularly relevant when the aim is to reduce metabolic cost, as to do so typically involves the measurement of noisy, low frequency calorimetric data, which requires large measurement times in order to produce accurate readings [40]. This presents two issues: first, as the time spent walking increases, so too does the likelihood that the subject will become fatigued. Not only is this uncomfortable for the subject, increasing the potential for early termination of the process, but due to physiological changes, which reduce the energy efficiency of fatigued muscles [41], further measurements cannot be considered valid. Second, long measurement times effectively place limitations on the complexity of the optimization objective. For example, relatively simple control profiles offering unimodal assistance patterns may be used [27], [28], albeit to strong effect. In order to explore the use of more complex control parameterizations, which may offer even greater energetic cost reductions, or to optimize the control of multijoint exoskeletons and exosuits, more efficient HIL optimization protocols are necessary.

This problem of excessive runtimes in HIL protocols is well recognised, and recent works have attempted to find solutions by implementing early-stopping within the optimization process [42] or by replacing the use of respiratory gas analysis with machine learning models on less coarse data inputs [43]. We propose an alternative approach, which leverages the strengths of musculoskeletal modeling [44]. Simulation-based approaches have proven useful both for the analysis of exoskeleton-assisted locomotion [45], [46] and the design of exoskeleton controllers [47]. Utilising dynamic models driven by musculo-tendon actuators [48]–[51] combined with models of muscle energetics [52], [53] the metabolic power consumption of movements can be readily estimated [47], [54], providing approximations to the ground truth data from calorimetry [53], [55]. Musculoskeletal models can easily be scaled to match a subject in terms of proportions, but adapting muscle parameters (for example, to differentiate between subjects with different muscle strengths) is challenging, and furthermore these models do not by themselves account for innate differences in walking styles. By combining musculoskeletal modeling with HIL optimization, we can efficiently simulate the metabolic cost of walking using a scaled generic model, while retaining the ability to learn personalized controllers using data collected directly from subjects.

To summarise, in this article, we present a HIL methodology, which optimizes the assistive torque patterns applied by exoskeletons. Musculoskeletal simulations are conducted online in order to simulate metabolic rate, significantly reducing the time investment required to sample specific torque profiles when compared to implementations relying on calorimetric measurements. We evaluate the effectiveness of our method for seven subjects wearing an active pelvis orthosis. In addition, we present results from a secondary investigation in to the correlation between simulated and experimental metabolic rate, based on data collected from three additional subjects wearing the same pelvis orthosis.

II. Hardware

A. Motion Capture Equipment

Our experiments were conducted in the Gait Lab, The University of Edinburgh, seen in Fig. 2. The lab is outfitted with a 12-camera motion capture system (Vicon, Oxford, U.K.) to track reflective marker trajectories as well as a six-axis, split-belt treadmill (Motekforce Link, Amsterdam, Netherlands) for measuring ground reaction forces and moments. The ground reaction force data is measured independently for each foot via two force plates integrated in to the treadmill, which report both forces and torques, i.e.,

$$\mathbf{f}_g = (f_x, f_y, f_z, 0, T_y, 0) \in \mathbb{R}^6 \tag{1}$$

as well as the centre of pressure on each force plate

$$\mathbf{c}_p = (c_x, c_y, c_z) \in \mathbb{R}^3 \tag{2}$$

where we have assumed that the vertical axis is in the y-direction. Note that twists in other directions could be introduced if vertical shear forces were present, e.g., when walking on unstable ground, however, this is typically not the case in treadmill walking.

Subjects also wore a Cortex Metamax 3BR2 system (Cortex, Leipzig, Germany) for a portion of the experiment, which was used to experimentally quantify the metabolic cost of walking.

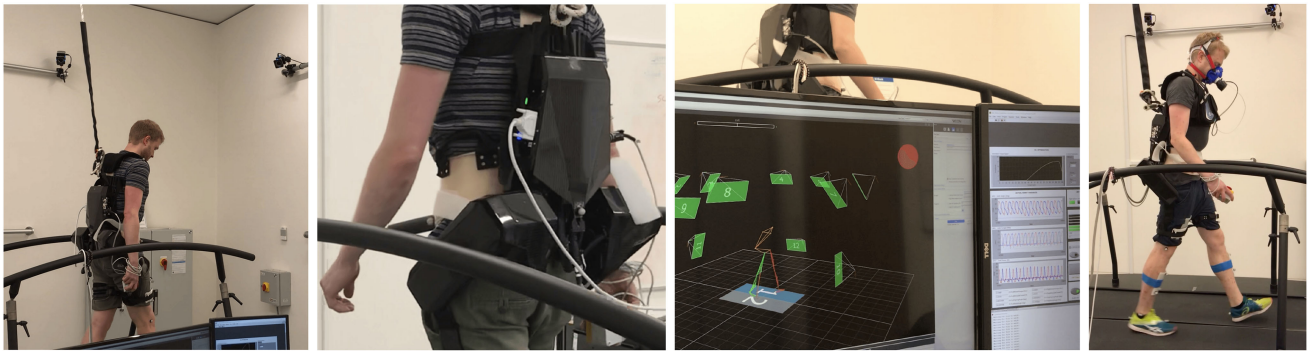

(a) (b) (c) (d)

Fig. 2. (a) Subject walking in the Gait Lab, The University of Edinburgh. Equipment shown includes a Vicon motion capture system, Motek Medical treadmill and active pelvis orthosis (APO). (b) Close-up of the APO worn by the same subject whilst walking. (c) Realtime capture of motion data via Vicon's Nexus software and the APO controller. (d) Subject walking whilst wearing a respiratory gas analysis device.

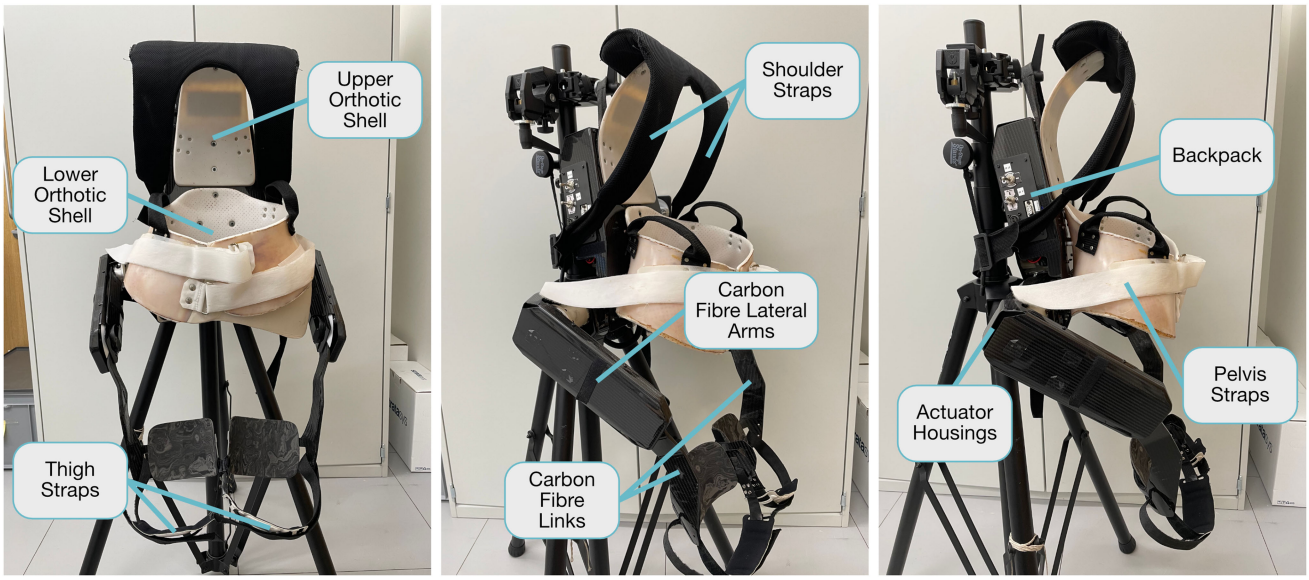

Fig. 3. Series of closeup images of the APO illustrating the various components, which comprise the device. Labels indicate the position of the orthotic shells, fastening straps, and the three main components of the exoskeleton itself: the backpack, actuator housings, and carbon fibre lateral arms.

The device takes breath-by-breath measurements of the rates of oxygen uptake and carbon dioxide output by the wearer. A subject is seen wearing the device in Fig. 2.

B. Exoskeleton System

During our experiments subjects wore the active pelvis orthosis (APO), a rigid pelvis exoskeleton, which is designed to offer flexion and extension assistance at the hip joint during walking [56]. This exoskeleton was developed at The BioRobotics Institute of Scuola Superiore Sant'Anna (Pisa, Italy); the technology is currently licensed to IUVO Srl (http://www.iuvo.company, Pontdera, Italy). The version of the APO used in this article is an evolution of an earlier design [56], which is now fully portable featuring an on-board battery with a total mass of 6.8 kg.

The physical structure of the APO consists of a backpack segment, which houses the battery and internal electronics; housings for the actuation units; two carbon fibre lateral arms, which contain a 4-bar power transfer mechanism [57]; and two carbon fibre links, which interface directly with the human thighs. Two orthotic shells attached to the backpack help to distribute the weight from the device evenly over the subject. The exoskeleton is secured to the wearer via a series of straps: one securing each thigh to the corresponding carbon fibre link, two straps securing the shoulders to the upper orthotic shell, and finally two further straps, which secure the lower orthotic shell to the pelvis. The components of the APO are labeled for reference in Fig. 3.

The APO is driven by two series elastic actuation units, which drive flexion and extension assistance on either side of the device [56]. Each actuator contains a 100 W dc motor in series with torsional spring of stiffness 100 Nm/rad. A harmonic drive and four-bar mechanism are used for gear reduction and power

TABLE I
APO TECHNICAL SPECIFICATIONS

Mass (kg)	Torque Limits (Nm)		Joint Limits (°)	
	Hardware	Software	Hardware	Software
6.8	±35	±15	$[-27°, 108°]$	$[-25°, 85°]$

transmission, respectively. More detail on the actuation system is provided by Giovacchini *et al.* [56]. Each actuation unit contains an absolute encoder, which measures the angle of each hip, as well as an incremental encoder, which measures the deflection of the torsional spring, which is used in combination with the known spring stiffness to compute the torque at each joint.

The APO is capable of producing a peak torque of 35 Nm [56], however, for safe and consistent operation a limit of 15 Nm of peak torque is recommended [57]. In our article, we found a limit of 10 Nm more suitable to maintain consistent operation of the device. The exoskeleton is controlled via a software interface built in LabView, which allows access to a low-level torque controller [56]. The absolute limits for extension and flexion angle of the carbon fibre links are $-27°$ and $108°$, respectively. However, software limits are in place to limit the range of motion to $[-20°, 85°]$ in practice for purposes of safety. The technical specifications of the APO provided in this section are summarized in Table I for ease of reference.

III. EXOSKELETON CONTROL

In this section, we introduce and list for reference the four high-level control modes used by the APO in this article.

A. Transparent Mode

In this mode, the APO commands a desired torque of 0 to its low-level PD controller $\tau_{\text{des}} = 0$ resulting in no assistance or resistance to the user as a result of the device's natural joint resistance [56].

B. Adaptive Oscillator Mode

Adaptive oscillator (AO) mode is designed to provide assistance to drive the wearer naturally towards their intended future joint angle. The APO applies an assistive torque according to the following relationship:

$$\tau_{\text{des}} = K_\nu(\theta(\phi + \Delta\phi) - \theta(\phi)) \tag{3}$$

where K_ν and $\Delta\phi$ are tunable parameters known as virtual stiffness and phase lead, respectively, ϕ is the current phase of the gait cycle, and θ is a function, which translates current phase in to an approximation of the current hip joint angle [56]. In other words, this control scheme applies torques proportional to the difference between current and future joint angles, where the future angle is determined by the phase lead, and the difference is scaled by the selected virtual stiffness. Adaptive oscillators [58] are used to estimate θ and ϕ from measured joint angles.

C. Human-in-the-Loop Mode

To employ the HIL approach for exoskeleton control, we require a parameterized control scheme for the APO. We define a generic assistance profile, which is constructed as a piecewise combination of sinusoidal curves linking four node points, $\mathbf{p} \in \mathbb{N}^4$, where $p_i \in (0, 100)$ and $p_i < p_{i+1}$ for $i \in \{1, 2, 3\}$. In order from p_1 to p_4, the node points correspond to the points in the gait cycle at which maximum extension, positive inflection, maximum flexion, and negative inflection occur, respectively. This generic profile is shown in Fig. 4(a). Mathematically, the control signal applied via the APO is a piecewise combination of sinusoids, which takes the following form:

$$u(x, \mathbf{p}) = \frac{1}{2}\begin{cases} \tau_e(\sin(g(x, \mathbf{p}) + \frac{\pi}{2}) - 1) & 0 \le x \le p_1 \\ \tau_e(\sin(g(x, \mathbf{p}) - \frac{\pi}{2}) - 1) & p_1 \le x < p_2 \\ \tau_f(\sin(g(x, \mathbf{p}) - \frac{\pi}{2}) + 1) & p_2 \le x < p_3 \\ \tau_f(\sin(g(x, \mathbf{p}) + \frac{\pi}{2}) + 1) & p_3 \le x < p_4 \\ \tau_e(\sin(g(x, \mathbf{p}) + \frac{\pi}{2}) - 1) & p_4 \le x \le 100 \end{cases} \tag{4}$$

where we define

$$g(x, \mathbf{p}) = \pi\begin{cases} \frac{(x+101-p_4)}{(100+p_1-p_4)} & 0 \le x \le p_1 \\ \frac{x-p_1}{p_2-p_1} & p_1 \le x < p_2 \\ \frac{x-p_2}{p_3-p_2} & p_2 \le x < p_3 \\ \frac{x-p_3}{p_4-p_3} & p_3 \le x < p_4 \\ \frac{x-p_4}{100+p_1-p_4} & p_4 \le x \le 100 \end{cases}. \tag{5}$$

Here, $x \in [0, 100]$ is the point within a gait cycle expressed as a percentage, while τ_e and τ_f define the magnitudes of the negative and positive peaks, respectively. These magnitudes are determined according to the following relationships:

$$\tau_e = c \tag{6}$$

$$\tau_f = \frac{2}{3}\tau_e. \tag{7}$$

The shape of the HIL control mode was based on sample data collected of subjects walking with the APO in transparent mode. With the node points $\mathbf{p}$ chosen appropriately in their respective domains the resultant trajectory approximates that of the normalized hip torque trajectories from the sample data, as shown in Fig. 4(b). However, the width of the node point domains were made sufficiently wide, as seen in the shaded regions of the x-axis in Fig. 4(a), in order to allow for significant deviation from these trajectories. The constant c in (6) was chosen based on feedback regarding comfort from subjects, while keeping in mind the hardware limitations of the APO. The conversion factor of $2/3$ between extension and flexion torque magnitude is an approximation of what is observed in human gait data [59].

Previous works have indicated that optimal assistance magnitude can vary significantly between individuals [27], which suggests it would be suitable to include assistance magnitude as a parameter in the optimization process. Our framework did not take this approach as fixing the torque profile magnitude allowed for the use of a more complex control curve shape without requiring a significantly higher dimensional parameter space, which in turn would require an increase in data collection

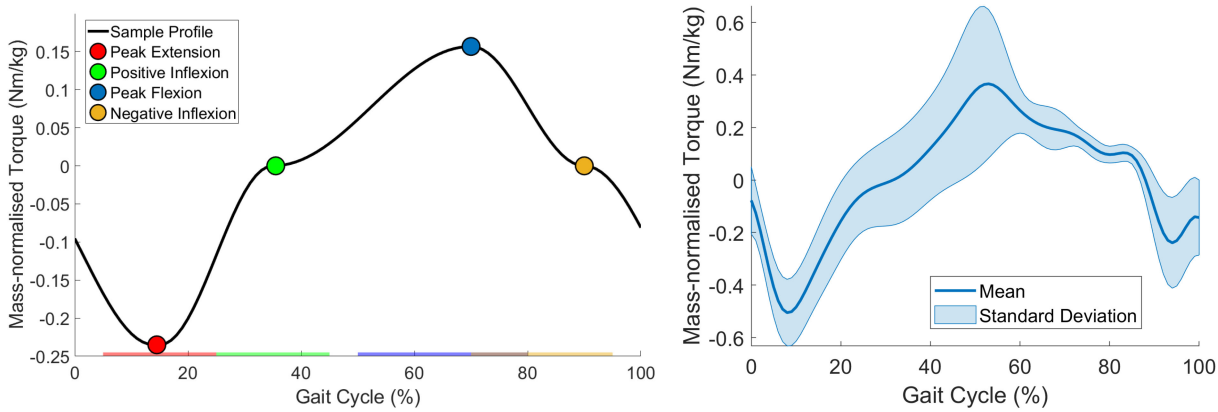

(a) (b)

Fig. 4. (a) Control parameterization utilised for this HIL study. The four parameters determining the shape of the assistance profile are represented by coloured dots. Each parameter has an associated allowable range, which is indicated by a shaded region on the x-axis. (b) Typical mass-normalized hip torque curve, with standard deviation, of transparent walking in the APO. This data corresponds to a total of 35 gait cycles from 7 subjects observed during steady treadmill walking, from an existing dataset of APO-assisted locomotion [46]. The parameterised HIL controller was designed so as to be able to approximate this trajectory whilst also allowing for significant deviations by varying the positions of the node points within the gait cycle.

times. Compared to two existing HIL implementations, which have focused on providing unidirectional assistance via two-dimensional (2-D) [28] or 3-D [27] control laws, this 4-D control law allows for a smooth transition between extension and flexion assistance.

D. Generic Mode

In this control mode, subjects receive two bursts of constant torque to assist flexion and extension of the hip. The parameters comprising this generic profile are based on a study in to the relationship between exoskeleton assistance timing and metabolic rate reduction in hip exoskeletons, which is discussed further in Appendix A. Extension and flexion assistance begins at 92% and 40% of the gait cycle, respectively, with each burst of assistance lasting for 25% of the gait cycle.

Mathematically, we can express the generic control signal as follows:

$$u(x) = \begin{cases} -\tau_e & 0 \leq x < 17 \\ \tau_f & 40 \leq x < 65 \\ -\tau_e & 92 \leq x \leq 100 \\ 0 & \text{otherwise} \end{cases} \tag{8}$$

where again $x \in [0, 100]$ is the point within a gait cycle expressed as a percentage, while τ_e and τ_f are as defined in Section III-C. The relationship between peak flexion and extension assistance specified in (7) was enforced to maintain consistency with the HIL control mode.

IV. Simulation Pipeline

A. Musculoskeletal Modeling

Our simulation framework utilises musculoskeletal modeling software OpenSim [44] in combination with a model designed for the evaluation of APO-assisted locomotion [46]. Musculoskeletal modeling is an increasingly widely used technique

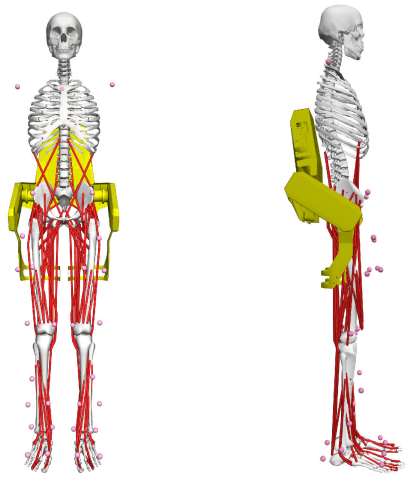

Fig. 5. Human-APO musculoskeletal model. The APO (shaded yellow) is constrained to the gait2354 model via weld joints. Model markers (shown in pink) are used to scale the model and perform inverse kinematics using experimental markers collected from motion capture.

in the computational biomechanics community; allowing for a wide variety of research studies in to human movement to be carried out in simulation [60]–[62].

The human-APO model, shown in Fig. 5, is based on the gait2392 model; a 3-D model of the human musculoskeletal system, which has been shown to accurately reproduce human gait patterns [63], [64]. For this article, we use a lower complexity version of the gait2392 known as the gait2354 model, which features 54 muscles, as opposed to 92 [65], resulting in lower computational overhead. The APO is constrained to this model via weld joints at the pelvis and at each thigh, forming the human-APO system model. The masses, inertia matrices, and geometrical features of the APO were obtained from CAD files provided by IUVO.

The generic human-APO model is calibrated for a particular subject via a scaling step, which minimizes the squared error between model markers and experimental markers from motion capture. The residual reduction algorithm is then used to account for discrepancies between the model and collected calibration data, which may result due to approximations in the model [44].

B. Motion Reconstruction

OpenSim uses the Simbody dynamics engine [66] to perform inverse dynamics by solving the multibody equation of motion over time, i.e.,

$$\tau = M(\mathbf{q})\ddot{\mathbf{q}} + \mathbf{C}(\mathbf{q}, \dot{\mathbf{q}}) + \mathbf{g}(\mathbf{q}) + J(\mathbf{q})^T f_{\text{ext}} \tag{9}$$

where τ and $\mathbf{q}$ are the vectors of joint torques and joint angles; M and J are the system mass matrix and Jacobian; $\mathbf{C}$ and $\mathbf{g}$ give the nonlinear and gravity terms; and finally f_{ext} is the net external force acting on the system, which typically in this case is due to a combination of ground reaction forces and exoskeleton assistance components.

Joint kinematics trajectories $\mathbf{q}(t)$ are obtained from experimental data via least squares minimization. The problem solved at each timestep is of the following form:

$$\min_{q} \sum_{i=1}^{m} w_i ||\mathbf{p}_i - \mathbf{x}_i(\mathbf{q})||^2 \tag{10}$$

where $\mathbf{p}_i$ is the 3-D position in space of the ith experimental marker and $\mathbf{x}_i$ is the 3-D position of the corresponding model marker, which is dependent on $\mathbf{q}$.

C. Static Optimization

The 23 degrees of freedom of the human-APO model are driven by 54 musculo-tendon units (MTUs). Each MTU produces force ϕ_m according to its current normalized lengths λ_m, velocities ν_m, and the level of muscle activation α_m, i.e.,

$$\phi_m = H(\alpha_m, \lambda_m, \nu_m, \pi_m). \tag{11}$$

Here, H is a black-box function, which encodes the relationship between generated muscle force, the current state of the musculoskeletal model, and a set of muscle parameters π_m. These parameters include both muscle-specific quantities, such as maximum isometric force, and subject-specific quantities such as optimal fiber length and tendon slack length. Muscle-specific quantities are as specified in the generic gait2354 model, while subject-specific quantities are calculated during the scaling step outlined in Section IV-A. The behavior of H depends on the muscle model used, which in this case is a modified version of a Hill-type muscle model [67], referred to within OpenSim as the Thelen 2003 muscle model. In practice, muscle forces are computed internally within OpenSim's static optimization tool via the MATLAB API, using the scaled model and input motion data for each subject.

Consider a time history of torques at each joint of the model, as computed by (9). These joint torques are composed of force contributions from the muscles of the model, which are mapped in to joint space by a coupling matrix C_m determined by the placement of the muscle relative to the joint [68]. For a given joint j with c muscles crossing that joint, we have

$$\tau_j = \sum_{m=1}^{c} \phi_m^{\top} C_m. \tag{12}$$

For a known set of joint torques there are infinitely many solutions for the corresponding muscle activations. To identify a unique solution, we can optimize over some objective function; in this article, we choose to minimize the sum of squared muscle activations, i.e.,

$$\min \sum_{m=1}^{n} (\alpha_m)^2, \tag{13}$$

where for our model we have $n = 54$. The process of solving (11) and 12 while minimising (13) is known as static optimization. Static optimization is significantly faster computationally than dynamic tracking algorithms such as CMC, and previous work has indicated that for relatively low-impact movements (e.g., walking) the differences in the obtained muscle activations are minimal [69], [70].

D. Muscle Energetics

Once the muscle activations are known, we employ a muscle energetics model to compute the energy expenditure for each muscle. The muscle energetics model used is based on the well-known model by Umberger [52] with modifications to the recruitment of muscle fibres and the treatment of mechanical work [53]. For simplicity we will again use a black-box function U to express this model

$$\dot{\epsilon}_m = U(\alpha_m, \lambda_m, \nu_m, \pi_m) \tag{14}$$

where $\dot{\epsilon}_m$ is the rate of energy usage of muscle m. Through summation over the full set of muscles we can compute the rate of energy usage of the entire model as

$$\dot{\epsilon} = \sum_{m=1}^{n} \dot{\epsilon}_m \tag{15}$$

where $\dot{\epsilon}$ can be seen as the overall energetic cost associated with the movement. In practice, computing muscle energetics in OpenSim is achieved via the use of a metabolics probe, which when added to a musculoskeletal model solves (14) for each muscle at each timestep of a recorded motion [53].

V. HIL Optimization Implementation

In this section, we will outline the specific components of our HIL protocol, particularly with reference to the schematic given in Fig. 1, which outlines the generic HIL optimization structure.

A. Real-Time Measurement

The real-time measurement in the protocol consists of marker trajectories and external forces collected in the University of Edinburgh Gait Lab. As part of the processing steps outlined in Section VI-E, the raw data is segmented in to synchronized gait

cycles.[1] Therefore, we have

$$\mathrm{P} = \{\mathbf{p}_1, \mathbf{p}_2, \ldots, \mathbf{p}_n\} \tag{16}$$

$$\mathrm{F} = \{\mathbf{f}_1, \mathbf{f}_2, \ldots, \mathbf{f}_n\} \tag{17}$$

where P and F contain marker and external force data, respectively, for n total gait cycles. Here, the external force data includes contributions from ground reaction forces as well as torques applied by the APO. Note that vectors in this section are indexed by time, i.e., $\mathbf{p}_1(t)$, but we leave this dependence implicit in order to simplify notation.

B. Performance Metric

In the context of this article, the APO is worn with the intent to reduce the metabolic cost of walking as much as possible. To this end, we use metabolic energy expenditure as our performance criterion for the HIL optimization, and aim to minimize this over the course of our protocol. To avoid the lengthy collection times associated with the use of calorimetry we instead simulate metabolic energy usage. This is done using the human-APO model introduced in Section IV-A alongside the simulation capabilities of OpenSim.

The performance metric calculation occurs over several steps. For each gait cycle, we first use the collected marker data to define the motion of the model via inverse kinematics (see Section IV-B)

$$Q = \{\mathbf{q}_1, \mathbf{q}_2, \ldots, \mathbf{q}_n\}. \tag{18}$$

Then, we use the modeled joint trajectories and the measured external forces to find the set of muscle activations, which correspond to this motion via static optimization (see Section IV-C)

$$\mathrm{A} = \{\alpha_1, \alpha_2, \ldots, \alpha_n\} \tag{19}$$

and compute the metabolic energy rate using a muscle energetics model (see Section IV-D)

$$\mathrm{E} = \{\epsilon_1, \epsilon_2, \ldots, \epsilon_n\}. \tag{20}$$

Next, we compute the normalized metabolic rate for each cycle. For the ith gait cycle, which begins at time t_{i-1} and ends at time t_i, we compute the rate of energy consumption, normalized by subject mass M, as follows:

$$V_i = \frac{1}{M(t_i - t_{i-1})} \int_{t_{i-1}}^{t_i} \dot{\epsilon}_i(t) dt. \tag{21}$$

The final step in our performance calculation is to average the simulated metabolic rate over all collected gait cycles

$$V_s = \frac{1}{n} \sum_{i=1}^{n} V_i. \tag{22}$$

We refer to V_s as the simulated metabolic rate. Note that, similar to the experimentally measured metabolic rate V_e introduced in Section VI-E, V_s expresses an approximation to the ground-truth normalized metabolic rate V.

[1]Here, we use the common definition of a gait cycle as beginning at heel-strike and ending at the subsequent heel-strike of the same foot.

C. System Update

The component of our system, which we seek to optimize is the assistive torque profile applied by the APO. We consider the parameterised control signal $u(x, \mathbf{p})$ defined in (4) with the following constraints placed on control parameter domains:

$$p_1 \in [5, 25] \tag{23}$$

$$p_2 \in [25, 45] \tag{24}$$

$$p_3 \in [50, 80] \tag{25}$$

$$p_4 \in [70, 95]. \tag{26}$$

These ranges were chosen to limit the search space for the optimization while still allowing for significant flexibility in the possible assistance patterns, and in particular were chosen so as to allow for assistance profiles, which mirror human joint torques [59].

D. Optimization Step

We employ the use of Bayesian optimization in order to drive the selection of control parameters between loops of the HIL protocol. Bayesian optimization is a method of identifying the minimum of a function $f : X \to \mathbb{R}$, for some bounded set X, where samples from f can be readily obtained. To do so, a model for f is created using Gaussian processes, and updated with the data from successive samples. The appropriate points in the domain at which to sample from are determined through the optimization of an acquisition function, which determines the most valuable point according to some criterion [71].

This optimization approach is particularly well suited to minimizing functions, which are expensive to evaluate, and as such has been used successfully in a number of previous HIL optimization protocols [28], [30], [31], which by their nature involve lengthy data collection steps. Here, the function we are aiming to minimize is the unknown relationship between the control parameters and the ground truth metabolic rate, i.e.,

$$V = f_s^C(\mathbf{p}). \tag{27}$$

Here, we use the subscript s to denote that the learned policy is specific to each subject and the superscript C to denote an underlying set of context parameters, such as walking speed and inclination, which may also affect this relationship.

Our optimization process is implemented in MATLAB using MATLAB's *bayesopt* function, which is an implementation of Bayesian optimization, and takes place over a total of 24 iterations. The first 12 samples are randomly selected within the domain, so as to avoid early convergence to a local minima, while the latter 12 follow from optimization of the *expected improvement* acquisition function [71].

VI. Experimental Design

We tested our HIL framework on 7 healthy subjects, comprising 5 males and 2 females, none of whom presented with gait pathologies. All subjects were adults between the ages of 22 and 34 and were volunteers from the students and staff of the School of Informatics, The University of Edinburgh. Healthy

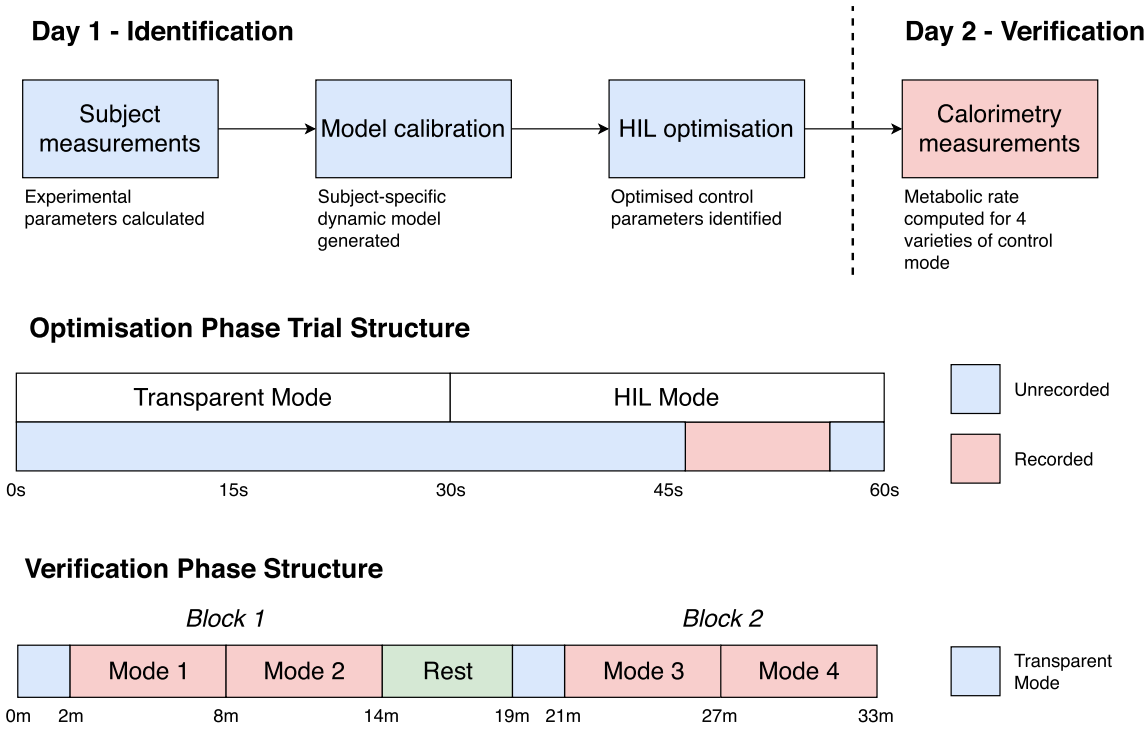

Fig. 6. Top: the sequence of steps which took place over the 2-day experimental protocol. Middle: the structure of a single walking trial within the HIL optimization step. The upper layer of the figure indicates whether the APO was in transparent or active mode, while the lower layer shows the period during which data was collected. Bottom: the structure of the verification phase, during which subjects walk whilst experiencing a number of APO assistance modes. The ordering of the four active assistance modes (red background) was randomized for each subject.

TABLE II
PHYSICAL AND EXPERIMENTAL SUBJECT PARAMETERS FOR HIL SUBJECTS

ID	Mass (kg)	Height (m)	Leg Length (m)	Stride Time (s)	Peak APO Torque (Nm)	Identification Mode
1	67.3	1.80	0.93	1.15	15.8	HIL
2	71.3	1.82	0.84	1.09	10	HIL
3	79.3	1.74	0.75	1.03	10	HIL
4	58.6	1.78	0.84	1.09	10	HIL
5	59.9	1.68	0.75	1.03	8	HIL
6	81.4	1.81	0.83	1.08	15	Grid Search
7	68.3	1.62	0.79	1.06	10	Grid Search

subjects of a young age were preferred in order to minimise the risk of fatigue affecting the results of the HIL algorithm. Ethical approval for the study was sought and granted from the School of Informatics Ethics Committee, The University of Edinburgh.

Our experimental protocol consisted of a model calibration step followed by two distinct phases: the parameter identification phase, in which subject-specific control parameters were identified, and the verification phase, in which the metabolic cost of walking with a number of control modes was evaluated for each subject. In order to avoid subject fatigue, these phases were conducted over a two day period. Fig. 6 illustrates the main steps, which took place over each day.

All subjects completed the same verification phase, however, for comparison purposes two subjects undertook an identification phase based on a simple grid sampling procedure, while for the remaining five subjects the HIL protocol outlined in Section VI-B was used. The search strategy employed for each subject is noted in Table II.

A. Model Calibration

Subject mass and leg length were measured at the beginning of the experiment and are presented in Table II. The baseline walking speed for each subject was determined according to the principle of dynamic similarity [72], as follows:

$$v = \sqrt{F_r g L} \tag{28}$$

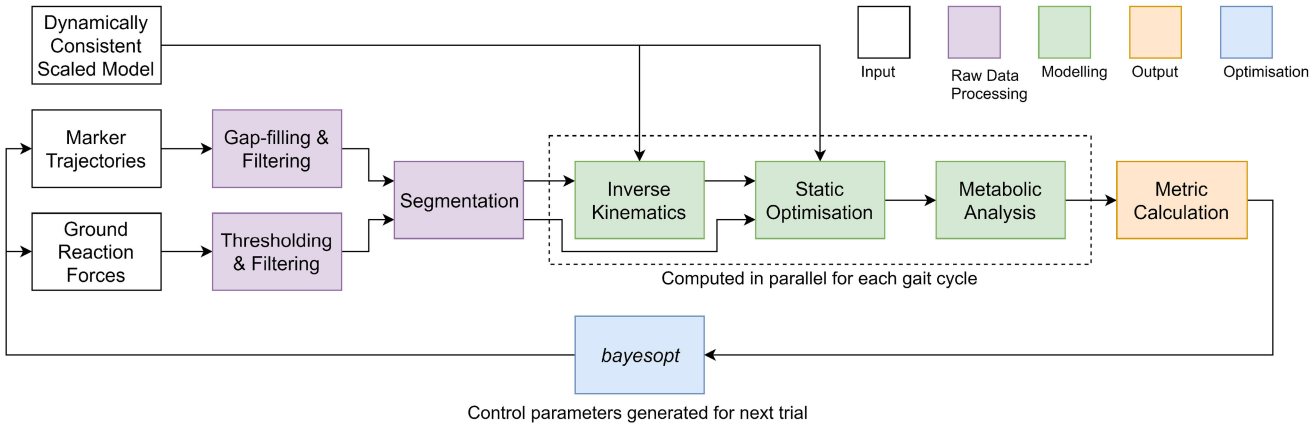

Fig. 7. Schematic outlining the structure of a single trial taking place during the identification phase. Raw data are collected and run through a series of processing steps, producing data for four gait cycles. The normalized metabolic rate is computed for each cycle and averaged to produce a single measurement for the trial. This measurement is input to the Bayesian optimization algorithm, which then suggests control parameters for the next trial.

where v is baseline walking speed, F_r is the Froude number (chosen here to be 0.1), g is gravitational acceleration, and L is leg length (measured as the vertical distance from the greater trochanter to the medial malleolus). All subjects were made to walk at a pace equivalent to 120% of their baseline walking speed.

During this step, marker data from a static pose was collected and used alongside subject mass to scale the generic human-APO musculoskeletal model for each subject. Participants then underwent a 60 s walk with the APO in transparent mode. Gait cycles from the latter 30 s of this transparent mode data were used to produce a dynamically consistent scaled model via the RRA algorithm [44], and to identify the preferred stride time for each subject, which was taken as the average time of stride across all gait cycles. The preferred stride times for each subject are presented in Table II.

B. HIL Parameter Identification

During the parameter identification step, subjects were partitioned in to two groups: those undergoing HIL-based sampling and those undergoing a simple grid search. The search strategy employed for each subject is noted for reference in Table II.

Subjects undergoing the HIL-based search strategy completed 24 consecutive walking trials, each of which corresponded to a single measurement for the optimization. Each trial lasted 60 s and consisted of 30 s walking in transparent mode followed by 30 s of assisted walking. Ten seconds of motion data was collected from the end of the assisted period, and used to compute the mean metabolic rate for each tested control parameterization. For reference, the trial structure described here is illustrated in Fig. 6. Subjects were given feedback in the form of a 4-s audio cue prior to any change in assistance mode, but after recording was completed for that trial.

The data processing pipeline for each trial is presented in Fig. 7. Up to eight gait cycles were selected from the 10 s of motion data collected in each trial. Using OpenSim's modeling algorithms (see Section IV), the model kinematics, muscle activations, and corresponding metabolic rates were computed. Due to the limited time available to complete the data processing, the MATLAB Parallel Processing Toolbox was employed to execute these modeling steps for each gait cycle in parallel. The normalized metabolic rate was then calculated before being passed to the *bayesopt* function to select the new control parameters.

The control parameters $\mathbf{p}$ were updated for each trial according to the optimization step outlined in Section V-D. The first 12 sets of control parameters were selected randomly, so as to avoid early convergence to a local minima, while the latter 12 were determined automatically by the Bayesian optimization algorithm. Subjects were given a 5 min rest period between the first and second block of walking trials. After 24 iterations the optimal control parameters identified for each subject were noted in preparation for the verification phase.

For subjects selected to undergo a grid search, the control parameters $\mathbf{p}$ were selected randomly from a coarse discretization of the full 4-D parameter space. In this case, since any set of control parameters were selected independently from the previous set, the trial structure outlined in Fig. 7 was simplified to 30 s of assisted walking per trial, of which 10 s were recorded. The optimal combination of control parameters was then estimated via GP regression on the resultant simulated metabolic rate data.

C. HIL Verification

The verification step is designed as a sanity check on the results of the parameter identification phase. We collect indirect calorimetry from all subjects walking with assistance from the APO in HIL mode, with the optimized control parameters identified during each subject's individual identification phase. This data are used to compute the steady-state approximation of metabolic cost as outlined in Section VI-E, which is widely used in literature where metabolic cost of movement is studied [9], [12], [73]. Then, we contrast this result with further indirect calorimetry measurements taken in other exoskeleton control

TABLE III
ASSISTANCE MODE ORDERING

ID	Mode 1	Mode 2	Mode 3	Mode 4
1	Transparent	HIL	Generic	-
2	HIL	Generic	Transparent	AO
3	Transparent	Generic	AO	HIL
4	Transparent	AO	HIL	Generic
5	HIL	Generic	Transparent	AO
6	Transparent	HIL	AO	Generic
7	Generic	HIL	AO	Transparent

Note: the AO mode measurement for Subject 1 was collected on a subsequent day due to an issue with the calorimetry hardware.

modes in order to objectively quantify the performance of the HIL-optimized control scheme.

The control modes utilized by the APO are outlined in a generic form in Section III. For reference, and more specifically, the control modes, which were evaluated during this phase are as follows.

1) Transparent mode.
2) AO mode.
3) Generic mode.
4) HIL mode, using subject-specific parameters identified via the optimization phase.

Subjects walked at the speed calculated during their parameter identification phase, and completed a 6-min walk per assistance mode in two blocks of 12 min each. The blocks were preceded by 2 min of warm-up walking in transparent mode, and were separated by a 5 min rest period. For reference, the structure of the verification phase is depicted in Fig. 6. Reference measurements of resting metabolic rate (RMR) and free walking metabolic rate were also obtained, immediately prior to the main verification phase procedure.

In order to reduce the potential effects of fatigue on the verification phase results, as well as minimize any potential bias from mode order, the sequence of the assistance modes was randomly determined for each subject at the beginning of their verification day. The generated sequences are reported for each subject in Table III. Modes 1–4 in the columns of Table III correspond to the same modes of the verification phase, as depicted in Fig. 6.

In addition to collecting quantitative metabolic data, participants were also asked to rate the assistance modes they experienced in terms of both comfort and assistance quality. This was done at three distinct points during the verification process.

1) After Block 1, comparing assistance modes 1 and 2.
2) After Block 2, comparing assistance modes 3 and 4.
3) Upon completion of the verification phase, comparing all four assistance modes.

The purpose of the first two questions was primarily to provide subjects with a reference point for the relative strength of each assistance mode, while the responses to question three are considered the final responses for each subject and are discussed in more detail Section VII. In addition to the assistance modes listed above, subjects were given additional options for each question in case the perceived difference in assistance or comfort between modes was so slight as to be insignificant. For reference, full details of questions posed to subjects in the verification phase questionnaire are presented in Appendix B.

D. Analysis of Simulated Metabolic Cost

A number of previous works have used musculoskeletal modeling to quantify metabolic cost [47], [53], [54]. At least one work has sought to validate simulated metabolic cost approximations with respect to the ground truth of calorimetry data [55], finding that in general simulated and experimental metabolic rate are well corrolated. However, such studies are typically concerned with human locomotion in isolation, without the additional complexity of human-exoskeleton dynamic interaction.

To quantify the accuracy of the human-APO musculoskeletal model in terms of metabolic cost approximation, an additional experimental setup was devised to allow the simulated and experimental estimates of metabolic cost to be directly compared. A total of three healthy subjects between the ages of 21 and 33, two male and one female, walked with assistance from the APO whilst experiencing three levels of exoskeleton assistance. For this experiment, subjects wore both the Vicon marker set and the calorimetry device, enabling both simulated and experimental metabolic cost to be computed simultaneously. The data collected from each subject included marker trajectories, ground reaction forces, torques applied by the exoskeleton, and respiratory measurements.

Model calibration was carried out, as discussed in Section VI-A, and subjects again walked at 120% of their baseline speed as calculated by (28). The physical characteristics of each subject are summarized in Table IV, along with details of the control mode and level of assistance experienced by each subject, as well as the ordering of assistance levels. To examine the relationship between model complexity and accuracy of simulated metabolic cost, two personalized musculoskeletal models were calibrated for each subject: one based on the gait2354 model and other the gait2392 model, both of which are lower-limb focused musculoskeletal models included within OpenSim. The gait2354 musculoskeletal model is an approximation of the gait2392 model intended to reduce the computation time of simulations [65].

Data was collected during four six min blocks (see Fig. 8). The collection protocol consisted of a RMR during quiet sitting followed by three active measurements of 6 min of calorimetry data. The active blocks were preceded by a warm up period of 2 min during which the APO was placed in transparent mode. A total of 3 min of motion capture data[2] was collected per assistance level.

E. Raw Data Processing

Marker trajectories and ground reaction force readings were collected at 100 and 1000 Hz, respectively. The marker and

[2]Here, motion capture data refers to marker trajectories and recorded forces, but not calorimetry data.

TABLE IV
PHYSICAL AND EXPERIMENTAL SUBJECT PARAMETERS FOR METABOLIC COST SUBJECTS

ID	Mass (kg)	Leg Length (m)	Control Mode	Assistance Level			Assistance Order		
				Low	Medium	High	Level 1	Level 2	Level 3
8	99.4	0.86	AO	10	15	20	Low	High	Medium
9	62.1	0.82	AO	5	10	15	High	Low	Medium
10	72.5	0.82	Generic	4	8	12	Medium	High	Low

Note: the meaning of the "Low," "Medium," and "High" parameters is dependent upon the active control mode. In the AO control mode, these parameters correspond to virtual stiffnesses, while in the generic control mode these correspond to the peak value of flexion assistance. Subject 9 required a reduction in virtual stiffness due to a failure of the AO algorithm to stay in phase at high stiffness levels.

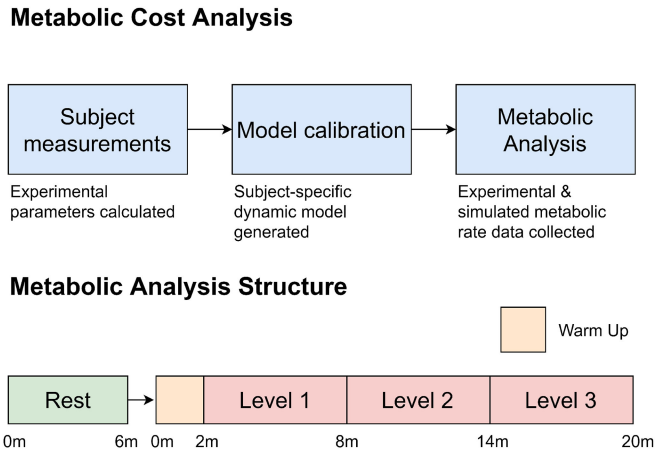

Fig. 8. Top: the overall structure of the experiment designed to investigate the accuracy of simulated metabolic cost as a surrogate metric for experimental metabolic cost. All steps were carried out as part of a 1-day experimental protocol. Bottom: a breakdown of the structure of the experiment. First, a rest measurement was taken from each subject during a period of quiet sitting. Then, subjects walked at three distinct levels of effort, while measuring both simulated and experimental metabolic cost. The ordering of the effort levels was randomized for each subject.

ground reaction force data streams were automatically time-synchronised via the use of a Vicon Lock+ box.

All marker data was first processed using Vicon's Nexus software with a combination of gap-filling algorithms and low-pass filtering at 6 Hz using a Butterworth filter. Custom code was developed to process the ground reaction force data using a sequence of thresholding and filtering steps, and to segment both the marker and ground reaction force data in to discrete gait cycles via stance phase detection.

Breath-by-breath measurements of oxygen uptake were obtained using the Cortex Metamax 3BR2 system. Each measurement was conducted over a 6 min period. The data from the first 4 min of each measurement was then discarded, leaving 2 min of usable data per measurement. Discarding the first 4 min ensures that the data used in subsequent calculations corresponds to a steady state of metabolic rate, which is necessary to account for the physiological delay between instantaneous and measured energetic cost [40], and is standard practice when dealing with experimentally measured metabolic rate data [9], [12], [73].

To compute the metabolic rate from this experimental data, we employ the following relationship from Brockway [55], [74]

$$V_e = \frac{4.184}{60}(3.972 + 1.078R)\dot{V}O_2, \tag{29}$$

where R is the respiratory exchange ratio and $\dot{V}O_2$ is the mean relative oxygen uptake measured in ml/min/kg, meaning V_e has units of W/kg. Note that here we have used a subscript to denote experimentally measured metabolic rate, which we consider to be an approximation to the ground truth metabolic rate V, which describes rate of energy consumption per unit mass. The experimentally measured metabolic rate, V_e, was averaged over the 2 min of usable steady-state calorimetry data to produce a single value per measurement.

VII. RESULTS

A. Human-in-the-Loop Optimization

All subjects successfully completed both stages of the experimental protocol. In Table V, the optimized control parameters identified for each subject are listed, along with the metabolic rates found in each tested mode of assistance during the verification phase. The RMR value for S1 is unavailable due to an error in the data collection during this period; similarly, the AO measurement for S7 was discarded due to a failure of the adaptive oscillator algorithm to synchronise with the gait of the subject.

An analysis of the statistically significant differences between subjects and control modes is presented in Fig. 9. Notably, only S1 and S5 experienced a significant difference between transparent mode walking and any of the other tested control modes; the modes in question being HIL mode for S1, and both HIL and generic mode for S5. The overall level of statistical difference between control modes, when averaged over groups of subjects, is presented in Fig. 10(a) and (b). Only the change in HIL mode metabolic cost was statistically significant when averaging over our entire cohort of subjects. The statistical analysis of calorimetry data was carried out via a one-way anova on the breath-by-breath calorimetry data, making use of a combination of MATLAB's *anova1* and *multcompare* functions.

The mean metabolic rates for each assistance condition are averaged over all subjects and are collated at the bottom of Table V. On average, only the generic and HIL-optimized controllers are able to reduce metabolic cost relative to transparent mode walking, though, as seen in Fig. 10(b), the difference in

TABLE V
OPTIMIZED CONTROL PARAMETERS AND METABOLIC RATE DATA

Subject ID	Control Parameters (% of Gait Cycle)				Experimental Metabolic Rate (Wkg^{-1})					
	p_{ext}	p_{rise}	p_{flex}	p_{fall}	RMR	Free Walking	Transparent	AO	HIL	Generic
1	9	26	50	88	-	4.56	5.98	5.89	**4.96**	5.42
2	5	32	71	75	2.13	4.57	4.75	**4.72**	4.74	4.75
3	5	26	76	83	1.81	4.54	4.35	4.40	4.26	**4.06**
4	5	31	51	84	1.47	4.66	4.81	4.91	**4.68**	4.86
5	18	27	75	80	1.20	3.42	3.70	3.61	**3.34**	3.35
6	10	30	65	75	1.35	4.11	4.48	4.66	**4.46**	4.65
7	5	26	50	80	1.50	3.84	**3.77**	-	3.90	3.98
Mean	8.14	28.29	62.57	80.71	1.58	4.24	4.55	4.58	4.35	4.44
Standard Deviation	4.85	2.63	11.98	4.75	0.34	0.47	0.77	0.74	0.55	0.69

Note: bold font is used to denote the assistance mode with the lowest measurement of experimental metabolic rate for each subject.

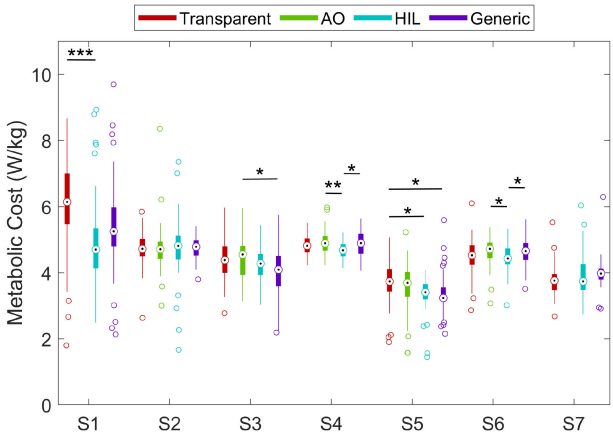

Fig. 9. Boxplot diagram illustrating the experimental metabolic rate measurements for each combination of subject and control mode. The central dot of each box corresponds to the median of the group, while whiskers convey the upper and lower quartile, and exterior circles denote outlier data points. Asterisks are used here to represent significant differences between groups, with $p < 0.05$, $p < 0.01$, and $p < 0.001$ represented by 1, 2, and 3 asterisks, respectively.

TABLE VI
PARTICIPANT QUESTIONNAIRE RESULTS

Subject	Most Comfortable	Best Assistance
1	N/A	N/A
2	Transparent	AO
3	HIL	HIL
4	HIL	Generic
5	HIL	HIL
6	Transparent	HIL
7	HIL	HIL

Note: answers to the participant questionnaire were not recorded for Subject 1.

generic mode is not statistically significant. Among those modes in which the subject is encumbered by the APO, the lowest absolute metabolic cost is incurred by the HIL-optimized control scheme.

The final responses from the participant questionnaire with regards to perceived comfort and assistance level are provided in Table VI. The number of subjects identifying each assistance mode as either most comfortable or the mode, which provided the best assistance is displayed in Fig. 11(a) and (b), respectively. From these graphs, we see that the HIL-optimized mode was the most likely to result in an assistance profile, which was perceived as comfortable and helpful amongst all assistance modes.

We found that the shape of the optimized assistive torques varied significantly between subjects. In Fig. 12(a), the mean optimized torque profile over all subjects is shown, alongside the individual torque profiles identified for each subject, while the standard deviation associated with each control parameter is provided in Table V. Our data suggests that the point of peak hip flexion moment (p_{flex}) in particular is the most susceptible to variations between subjects, exhibiting more than twice the error range of any other parameter. Meanwhile, the rising point of inflection (p_{rise}) is the control parameter, which exhibits the least variance.

Convergence is difficult to quantify for Bayesian optimization protocols, due to a tendency for the algorithm to balance exploring areas of the objective function, which are either high variance or near the currently expected minimum. In Fig. 13(a), we display the evolution of the iteration at which the minimum value of simulated metabolic cost was achieved. This quantity indicates how many iterations have passed since the Bayesian optimization has successfully sampled a lower point of the objective function, i.e. found a control parameterization resulting in lower metabolic rate, in this case. From this figure, we see a leveling off of the minimum index trace for each subject, which ranges from iteration 6 at the earliest for S5 to iteration 18 at the latest for S4. A more detailed example evolution of control parameters is shown for a specific subject in Fig. 13(b).

B. Simulated Metabolic Cost

All subjects completed the experimental protocol without issue, meaning the full 6 min of calorimetry data and 3 min of motion capture data was collected for each combination of

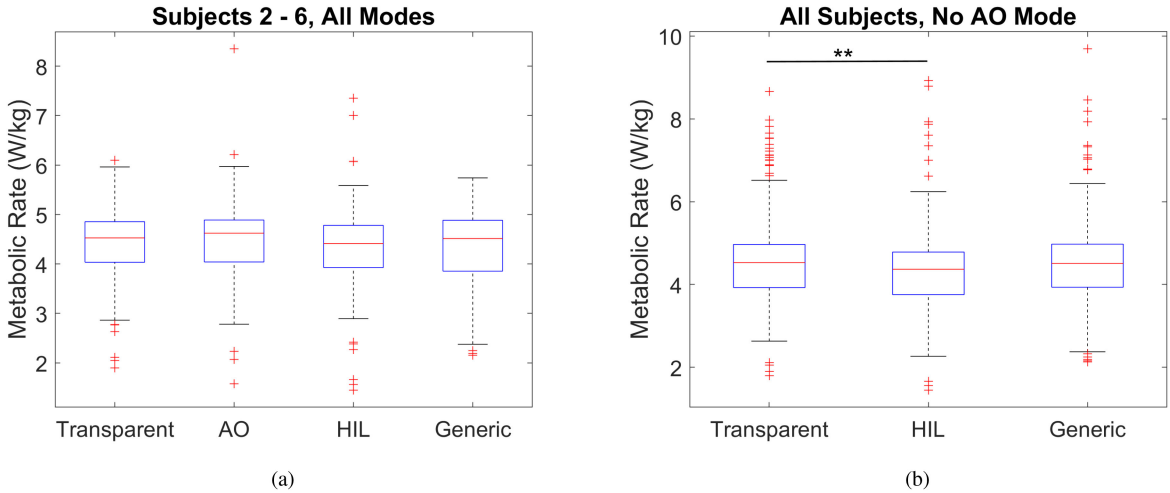

(a) (b)

Fig. 10. Boxplots illustrating the behavior of the verification phase data averaged over subjects. Here, the median value for each measurement is indicated by a red line. (a) Data from Subjects 2–6 averaged over all tested assistance modes. (b) Data from all subjects, averaged over the transparent, HIL and generic control modes. The asterisks indicate a significant difference with $p < 0.01$.

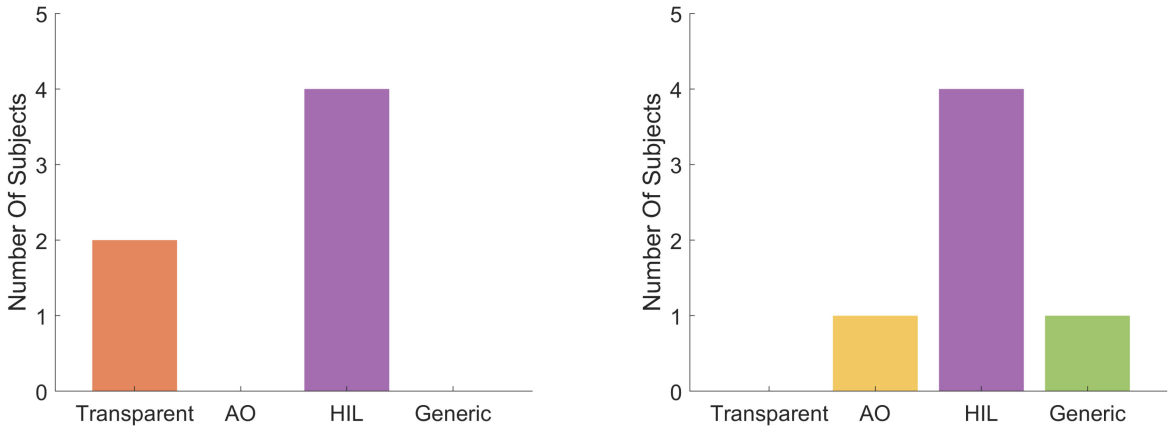

(a) (b)

Fig. 11. (a) Number of subjects who selected each APO control mode as the most comfortable. (b) Number of subjects who selected each APO control mode as providing the best level of assistance.

assistance level and subject. In Fig. 14, the simulated and measured metabolic rates are shown for each subject. For reference purposes, recordings of APO torques collected from S2 and S3 are displayed in Fig. 12(b), to provide a visualization of the AO and generic control modes.

In our results, simulated metabolic rate significantly overestimates the ground truth metabolic cost for all subjects, though to a lesser degree for S3 than S1 or S2. Metabolic cost is slightly lower when simulated using the gait2392 model compared to the gait2354 model, however, the general trend over effort levels is consistent between both models. Both methods for estimating metabolic cost are similarly noisy for S1 and S2, whereas for S3 simulated metabolic cost is significantly less noisy than experimental metabolic cost. This perhaps suggests that the generic control mode leads to a more consistent gait pattern than the AO control mode. In general, the relationship between metabolic cost and effort level is captured most accurately by the simulation methods for S2. For S1, the simulation-based approach incorrectly categorizes Effort Level 2 as the most energy efficient while according to the experimental measure this level incurred the highest energy cost. The relationship for S3 similarly was not captured by the simulation measures, though this subject exhibited a particularly minimal difference in experimentally measured metabolic cost between assistance modes, perhaps suggesting that the generic control mode was not effective at any magnitude for this subject.

VIII. Discussion

A. Human-in-the-Loop Optimization

The HIL-optimized control scheme, which results from our framework performs favourably compared to the two other

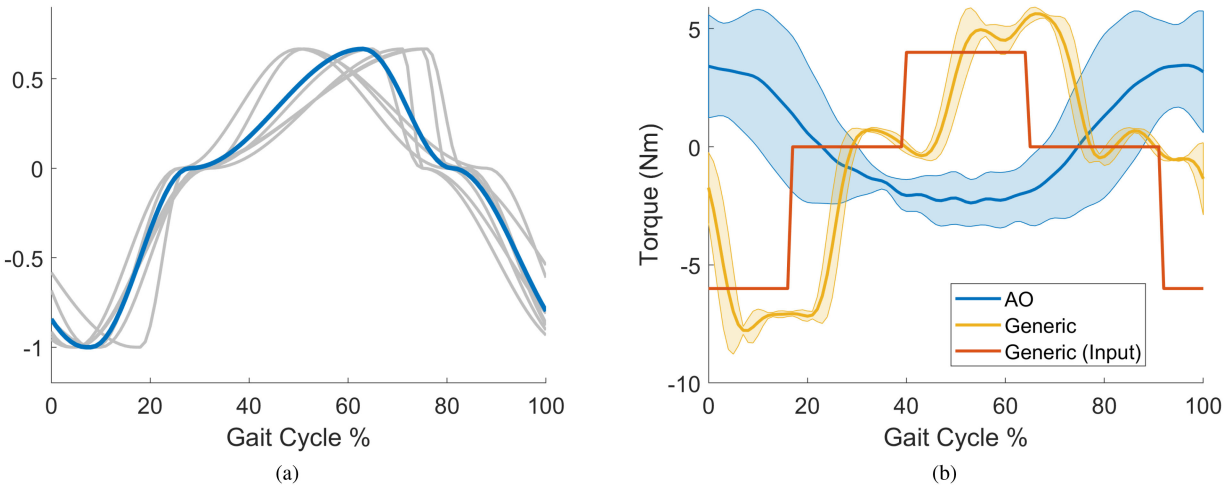

Fig. 12. (a) Mean control profile (blue) obtained by averaging the obtained control parameters over all subjects, overlaid with the standard deviations (red) of each control parameter at the corresponding node points. To illustrate the range of assistance profile shapes, each individual optimized profile is also shown (light grey) with extension magnitude normalized to 1. (b) Recordings of torques applied by the APO during the metabolic cost experiments. The applied torque trajectories for the AO and Generic control modes are shown, for S2 and S3 respectively, averaged over five gait cycles. The generic torque profile commanded to the APO is shown in red. Both samples were taken from Level 3 of the assistance order for each subject.

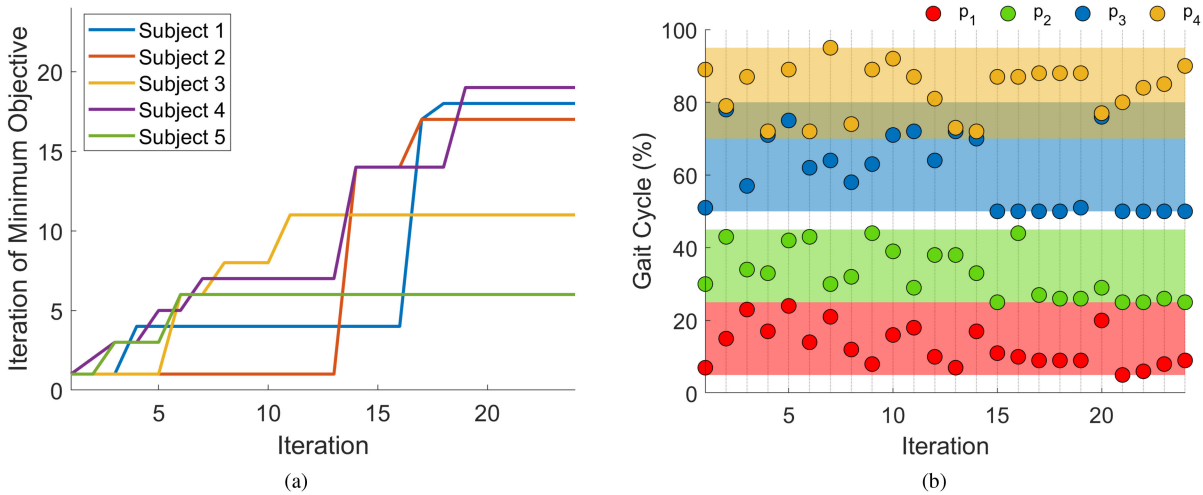

Fig. 13. (a) Trace of the iteration at which the minimum objective value was observed for each subject undergoing HIL-optimization via Bayesian optimization. Note that Subjects 6 and 7 are not included as their parameter identification phase relied on a grid search. (b) Diagram showing a sample of control parameter evolution for a single subject (S1). Shaded regions show the allowable values for the corresponding parameter. The random selection of control parameters is evident in the first 12 iterations, after which point the Bayesian optimization algorithm begins to converge towards a solution.

active controllers, and is the only control mode, which results in a statistically significant reduction in metabolic cost when compared to transparent mode walking, as shown in Fig. 10(b). However, our results also indicate that the efficacy of the exoskeleton control modes is highly affected by variations between subjects. To better illustrate the relative performance of the tested control schemes, we treat the cost of transparent-mode walking as a baseline and calculate relative reduction in energetic cost for the AO, generic, and HIL controllers. These results are displayed in Fig. 15 for Subject 1 and Subject 5. We observe that the metabolic benefit of the AO control scheme is minimal in both cases. Meanwhile, the generic control scheme offers a marked reduction in metabolic cost of approximately 10% when compared to the baseline for both subjects. We find that using the subject-specific control parameters identified by our optimization, we are able to further improve energy efficiency by a factor of 1.86 when compared to the generic controller for S1, compared to no relative gain for S5.

Though the generic mode performs similarly for S1 and S5, the results are quite different across the remainder of our dataset, and indeed the generic control mode results in increased metabolic cost for S4, S6, and S7. Comparatively, the HIL-optimized mode results in decreased metabolic cost for all subjects except S7. This is an interesting and quite unexpected result—the generic control mode was initially expected to perform fairly well for most or all subjects, being based on

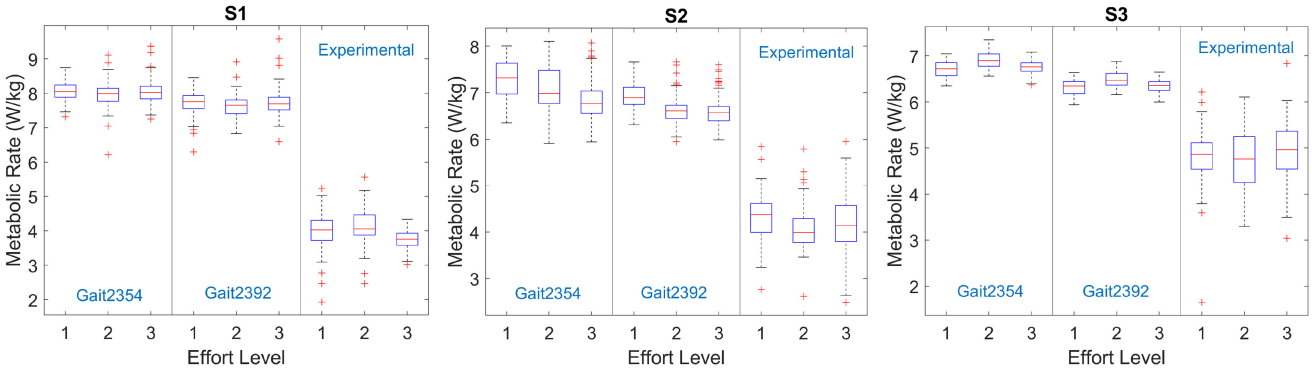

Fig. 14. Series of boxplots depicting results from the comparison between simulated and measured metabolic cost for all 3 subjects. The effort levels 1–3 are ordered as listed in Table IV. Metabolic rate was calculated in simulation using both the gait2354 and gait2394 models, as well as indirectly from calorimetry data. Labels in blue indicate the columns of each graph which relate to each calculation method.

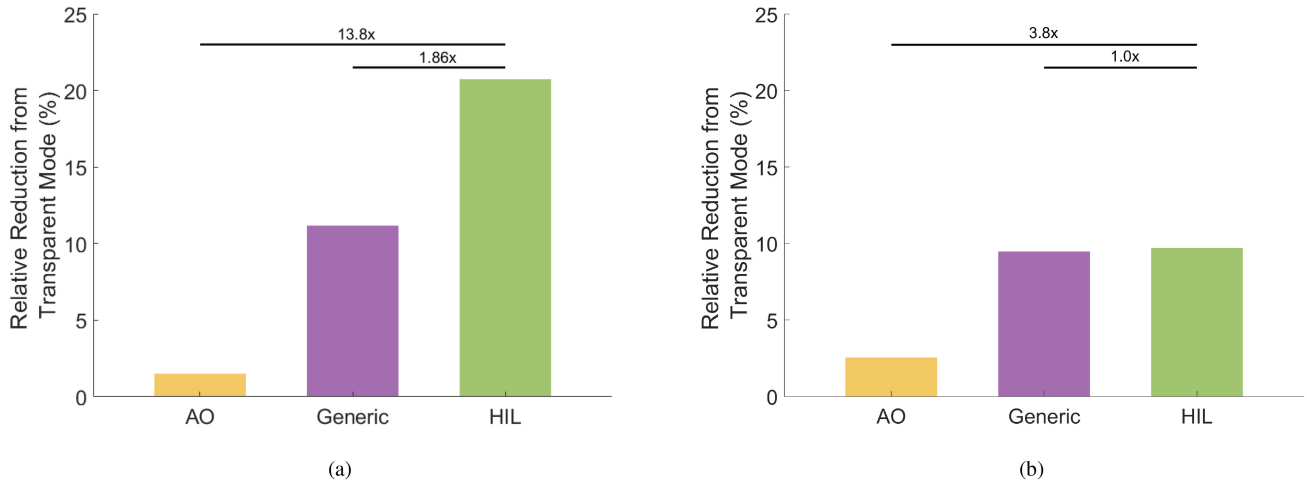

Fig. 15. Relative reduction in metabolic rate of the active control modes for (a) S1 and (b) S5, expressed as a percentage of the energetic cost of walking in transparent mode. Labels indicate the relative magnitude of reduction between modes.

a controller, which was optimized to be effective on a group level [20]. The poor performance of the generic mode over a portion of our dataset may indicate that the optimal exoskeleton assistance strategy is even more sensitive to subject parameters than was expected. Meanwhile, the poor performance of the HIL mode for S7 could be as a result of the grid search algorithm used to identify the control parameters for this subject, though it should be noted that the generic control mode also performed poorly. More data are required to quantify the relative importance of the Bayesian optimization driven search algorithm, however, a key advantage of this approach when compared to grid search methods is scalability to higher dimensions of control parameterization.

An interesting point of note is that subjects of similar mass and assistance level can exhibit markedly different results for each of the tested assistance modes. This is clear when comparing the results for, e.g., the HIL-optimized and generic modes for S4 and S5. Typically, human-in-the-loop optimization protocols use force and torque magnitudes which are fixed or scaled relative to subject mass. These results suggest that a more appropriate approach may be to include the maximum torque as an optimization parameter. It is likely that this would require too significant of a time investment for traditional HIL frameworks, which rely on calorimetry; however, this may be an interesting source of future work for our simulation-based framework.

While our HIL framework shows a statistically significant improvement compared to transparent walking, none of the tested control modes were able to consistently exceed the energy efficiency of walking without the exoskeleton over multiple subjects. Bettering the energy efficiency of not only transparent walking but free walking also is a difficult challenge, especially for a hip exoskeleton with on-board actuation and, thus, higher mass than, e.g., a soft exosuit. Nevertheless, ultimately the goal of exoskeletons for metabolic assistance is to improve the energy efficiency of walking in absolute terms, and so further work is required to improve the relative metabolic cost benefits of our approach.

The differences in optimized control strategies seen in Fig. 12(a) are likely due in part to the natural variations occurring between subjects, both in terms of the physical characteristics

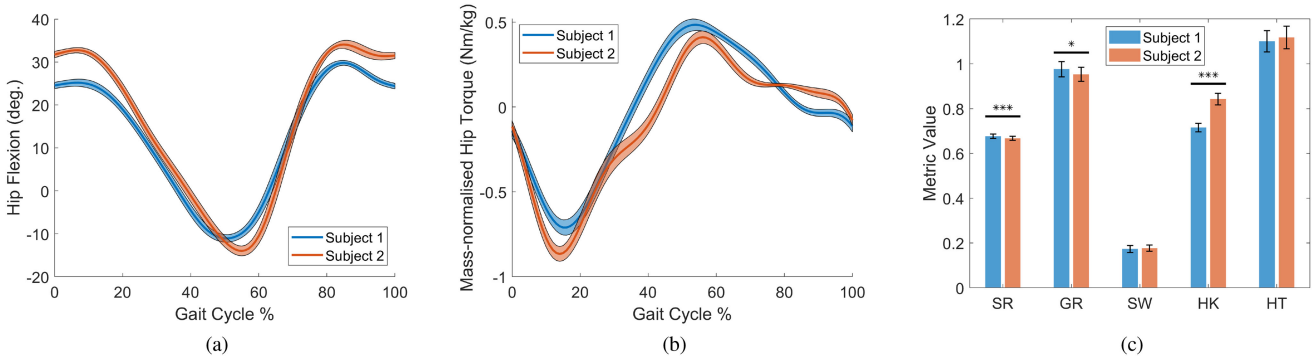

Fig. 16. Comparison of gait data between Subject 1 and Subject 2. These plots were obtained from data collected during the model calibration phase, which corresponds to 30 s of walking in transparent mode. (a) Mean and standard deviation of hip flexion/extension kinematics. (b) Mean and standard deviation of hip flexion/extension moments, normalized by subject mass. (c) Comparison of a range of gait metrics - stance ratio (SR), GRF peak ratio (GR), step width (SW), hip flexion/extension range of motion (HK), normalized peak to peak hip torques (HT). Asterisks denote a p-value of 0.001 and 0.05 for 3 asterisks and 1 asterisk, respectively.

listed in Table II and in specific locomotion strategies. To elucidate these internal differences, a sequence of diagrams is provided to compare and contrast various aspects of gait between two of the participants. In Fig. 16(a) and (b), respectively, we compare the hip kinematics and mass-normalized hip torques between Subject 1 and Subject 2, as measured during transparent walking while wearing the APO. In Fig. 16(c), we use the same dataset to compare a range of kinematic and dynamic gait metrics between the two subjects. These subjects were chosen as S1 experiences the most benefit from exoskeleton assistance, compared to S2 who experiences almost no change in any mode according to the values in Table V. The metrics tested include stance ratio, GRF peak ratio, step width, hip flexion/extension range of motion, and peak-to-peak hip torques (see Appendix C for a more thorough description of these gait metrics). We find statistically significant differences in 3 of the 5 tested gait metrics, indicative of a disparity in underlying locomotion strategies, but note no significant difference in peak-to-peak hip torques or step width.

Although the primary objective of this article was to target metabolic cost reductions, the postexperiment questionnaire results [see Fig. 7(a)] indicate that our control parameterization was both comfortable and gave the perception of increased assistance. It is particularly notable that no other active control mode was selected as the most comfortable. Although previous work has shown that subject perception does not necessarily match true metabolic cost [20], it is likely that subject comfort would be an important factor in promoting adherence to rehabilitation regimes or exoskeleton assistance programs, especially if the subject required assistance for extended periods of time. Therefore, increased comfort is a desirable characteristic.

Thus far, the focus of this article has been on collecting data from healthy participants, with a view to targeting exoskeleton assistance for metabolic rate reduction. For people who deviate significantly from normal gait patterns, such as those with gait pathologies, exoskeleton controllers based on datasets of healthy subjects are more likely to interfere with their walking style. Therefore, the personalized control schemes generated by HIL frameworks such as ours may be even more beneficial. Our framework, while implemented here using metabolic cost as the objective function, could be easily extended to further use-cases due to the depth of analysis enabled by the musculoskeletal modeling approach. For example, rather than looking at metabolic rate as a whole, physiotherapists could select specific muscles to target for assistance or training, depending on the needs of the subject. Such muscles could include deep muscles, which are hard to target experimentally (e.g., via EMG sensors).

B. *Simulated Metabolic Cost*

A potential weakness of our approach to the HIL optimization framework is a reliance on modeling assumptions, which are not present in traditional HIL protocols. The results discussed in Section VII-B suggest that modeling accuracy was to some degree dependent on both subject kinematics and the control mode applied.

A potential explanation for the discrepancies in simulated metabolic cost lies in the incomplete personalization of musculoskeletal models. In Section IV-C, we noted that the muscle parameters π_m include a mix of muscle-specific and subject-specific quantities. As a result of the scaling step mentioned in section IV-A, the musculoskeletal models used in this article were to some degree personalized for each individual subject. However, due to the challenge of directly measuring muscle properties from each subject, some muscle parameters, e.g., maximum isometric force, retained their generic values. Consequently, it is possible that the simulated metabolic cost was over or underestimated for subjects which significantly deviate from the physiological measurements on which the gait2392 and gait2354 models are based [65]. An interesting source of further study would be to investigate the sensitivity of our HIL optimization framework to these muscle-specific parameters; conducting a more detailed functional calibration for each subject could result in more personalized musculoskeletal models, which compute metabolic cost more accurately, and hence, perform better in our framework.

Additional tuning of musculoskeletal model parameters is likely to be necessary for subjects with pathological gait; recent

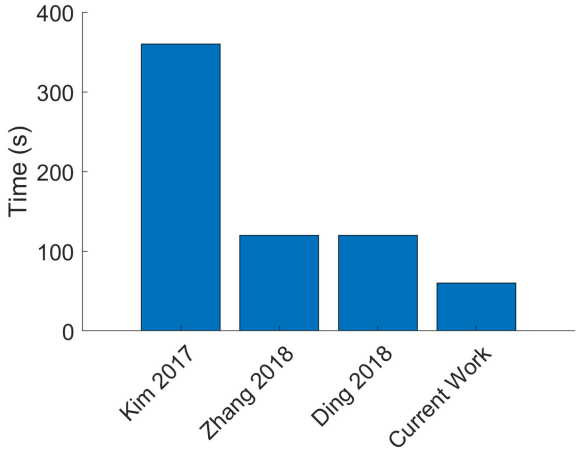

Fig. 17. Aomparison of the time taken per individual measurement between a number of recent HIL works [27], [28], [30] and the approach presented in this article ("Current Work").

studies have identified sensitivities to muscle parameters in both metabolic cost estimates of poststroke gait [75] and contact forces in the knee of an amputee walking with a prosthesis [76]. An additional source of further work for our framework will be to investigate the potential of musculoskeletal model calibration techniques [77] in combination with alternative objective functions, with the aim to recruit patients with gait pathologies. The input of a doctor or physiotherapist would be valuable in such cases to ensure that any modifications to muscle parameters are appropriate for the physiology of the subject.

C. Computational Efficiency

A key motivation for pursuing a human-in-the-loop optimization protocol with a simulated objective function was the potential benefit in terms of time investment. The results we have presented here involve only 60 s per iteration of the HIL process, compared to at least 120 s, but often longer, for methods based on calorimetry [26]–[30].

Total time of a HIL protocol is dependent upon factors like complexity of control parameterization and number of initial seed parameters, so it is difficult to directly compare this metric between studies. However, the length of an individual trial or measurement—for example, a single measurement of metabolic cost—is directly comparable. As set out in Fig. 6, the time required for each of our measurements was 60 s. In Fig. 17, we compare this trial time to a number of other recent studies, which have investigated the use of HIL optimization to reduce metabolic cost [27], [28], [30]. Our approach is more time-efficient than existing protocols, even where a more complex metabolic cost approximation method is used to shorten data collection times to 2 min [27], [28].

The 60 s required for our measurements can be further decomposed in to four phases: acclimatization, recording, raw data processing, and OpenSim processing. Acclimatization and recording times were fixed at 15 and 10 s, respectively. The total time for raw data processing (in Vicon's Nexus software) and OpenSim analysis (solving for inverse kinematics and subsequently static optimization) did not exceed 35 s, aided by the use of MATLAB's Parallel Processing Toolbox in combination with a high-spec computer processor (Intel(R) Core(TM) i9-9900KF, 3.60 GHz, 8 cores).

It should be noted that aspects of our HIL protocol involve additional overhead in terms of offline computation, e.g., initial scaling and calibration of musculoskeletal model, which does extend the total time taken. Crucially, however, subjects are not required to walk or otherwise generate data during this time, and so this does not incur any additional fatigue. A drawback of our approach is the requirement for a computer processor, which is sufficiently powerful to run static optimization at the required speed.

IX. Conclusion

In this article, we have presented a framework for optimizing exoskeleton control strategies based on a combination of musculoskeletal modeling and human-in-the-loop optimization. By leveraging the strengths of both approaches, our method can produce assistance strategies, which outperform generic controllers while requiring less time investment (particularly for participants) than recent state-of-the-art human-in-the-loop optimization methods. This is critical if these approaches are to be used for those with injuries or gait pathologies, where long experimental protocols are not an option, and so that increasingly complex control parameterizations can be investigated. Our method could also be useful for labs with motion analysis equipment and experience in musculoskeletal modeling, but without the ability to measure metabolic rate via calorimetry.

The results presented here further highlight the sensitivity of exoskeleton assistance strategies to differences between subjects, be they resulting from physical differences in height or limb length (for example), or variation in internal locomotion strategies. Even off-the-shelf control schemes, which have previously exhibited strong performance on the group-level were detrimental to the walking efficiency of some of our subjects. This highlights the need to identify personalized control strategies, which work well on an individual level—indeed, this is the primary strength of pure human-in-the-loop approaches. This need is, again, even more pertinent for those with gait pathologies, whose walking patterns are likely to be further removed from the normal trajectories on which many generic assistance controllers are based.

Further work remains to be done on the combined approach of musculoskeletal modeling and human-in-the-loop optimization, particularly to improve the accuracy of modeling human-exoskeleton interaction, and to explore alternate search strategies. However, we believe that this intersection of fields has a great potential benefit for the growing community of people who benefit from assistive robotic devices.

Appendix A
Generic Assistance Profile

The form of the generic assistance mode used in this investigation is based on a previous study in which the authors

investigated the effect of assistance onset timings on the performance of a hip exoskeleton [20]. A range of possible onset timings for hip flexion and extension assistance was tested on a set of 10 healthy subjects. They found that on average the combination of timing parameters, which reduced metabolic rate most effectively was 92.2% for the onset of hip extension assistance and 40.2% for the onset of hip flexion assistance. The duration of applied assistance was 25% for both flexion and extension. This particular study was chosen over similar alternatives [18], [19], [21] due to similarities in exoskeleton hardware (i.e., use of a rigid pelvis exoskeleton).

Appendix B
Questionnaire Format

As part of the verification phase outlined in Section VI-C, subjects were asked a series of questions regarding the perceived level of assistance and comfort offered by the tested control schemes. Subjects were asked to compare the control modes immediately after each block of the verification phase (see Fig. 6) and once again after completing the full experiment. For reference purposes, the full series of questions posed in the questionnaire is reproduced below.

1) *You have just experienced Assistance Mode A followed by Assistance Mode B.*
   a) *Which of the two modes, if either, did you find most comfortable?*
      1) *Mode* _ ii) *Both the same* iii) *Not sure*
   b) *Which of the two modes, if either, do you think best assisted your walking?*
      1) *Mode* _ ii) *Both the same* iii) *Not sure*
2) *You have just experienced Assistance Mode C followed by Assistance Mode D.*
   a) *Which of the two modes, if either, did you find most comfortable?*
      1) *Mode* _ ii) *Both the same* iii) *Not sure*
   b) *Which of the two modes, if either, do you think best assisted your walking?*
      1) *Mode* _ ii) *Both the same* iii) *Not sure*
3) *You have now finished the verification phase of the experiment. You experienced four assistance modes in the order A, B, C, D.*
   a) *Which of the four assistance modes, if any, did you find most comfortable?*
      1) *Mode* _ ii) *No one mode was best* iii) *Not sure*
   b) *Which of the four assistance modes, if any, do you think best assisted your walking?*
      1) *Mode* _ ii) *No one mode was best* iii) *Not sure*

Appendix C
Gait Metrics

Gait metrics are commonly used to assign quantitative measures to recorded gait patterns [46]. In Section VII, we compare the values of 5 kinematic and dynamic gait metrics between two subjects. The metrics used along with their definitions are as follows.

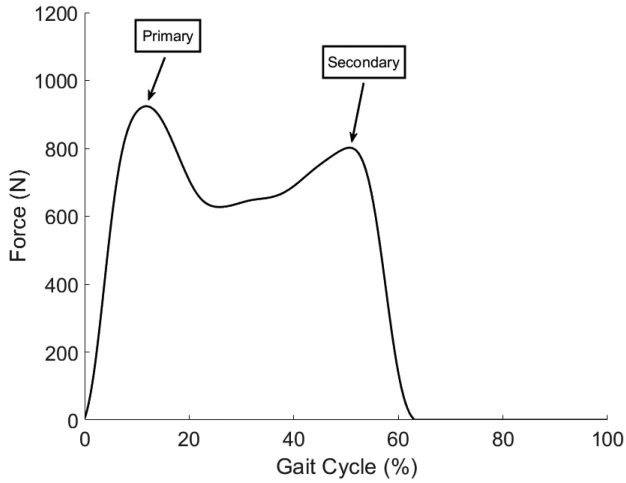

Fig. 18. Example trajectory of vertical ground reaction force of the leading foot over a gait cycle. The locations of the primary and secondary force peaks used in the calculation of the GRF peak ratio gait metric are shown.

1) Step width is defined as the medial-lateral distance between the heel of the subject at consecutive heel strikes.
2) Stance ratio is defined as the proportion of the gait cycle in which the leading foot is in stance.
3) GRF peak ratio is the ratio between the primary and secondary peaks of the vertical ground reaction force of the leading foot (see Fig. 18).
4) Hip flexion/extension range of motion is the absolute difference between the points of maximum and minimum hip flexion.
5) Peak-to-peak hip flexion/extension torque is the absolute difference between the maximum and minimum hip flexion torque, normalized to subject mass.

Acknowledgment

The authors would like to thank N. Vitiello and members of IUVO Srl, in particular Francesca De Simio, for providing extensive hardware support for the APO throughout the experimental data collection process, like to thank G. Henderson, for his contributions to the experimental setup and sharing of expertise on gait analysis, and Calum Imrie, for volunteering several times as a test subject during the initial design and refinement of the experimental protocol, and also like to thank the Human Performance Science Research Group, The University of Edinburgh, in particular Jon Kelly and Tony Turner, for sharing expertise with regards to human performance evaluation and providing training on the use of calorimetry equipment.

References

[1] A. M. Dollar and H. Herr, "Lower extremity exoskeletons and active orthoses: Challenges and state-of-the-art," *IEEE Trans. Robot.*, vol. 24, no. 1, pp. 144–158, Feb. 2008.
[2] T. Yan, M. Cempini, C. M. Oddo, and N. Vitiello, "Review of assistive strategies in powered lower-limb orthoses and exoskeletons," *Robot. Auton. Syst.*, vol. 64, pp. 120–136, 2015.

[3] S. Jezernik, G. Colombo, T. Keller, H. Frueh, and M. Morari, "Robotic orthosis lokomat: A rehabilitation and research tool," *Neuromodulation: Technol. Neural Interface*, vol. 6, no. 2, pp. 108–115, 2003.

[4] K. Y. Nam, H. J. Kim, B. S. Kwon, J.-W. Park, H. J. Lee, and A. Yoo, "Robot-assisted gait training (lokomat) improves walking function and activity in people with spinal cord injury: A systematic review," *J. Neuroeng. Rehabil.*, vol. 14, no. 1, pp. 1–13, 2017.

[5] M. P. De Looze, T. Bosch, F. Krause, K. S. Stadler, and L. W. O'Sullivan, "Exoskeletons for industrial application and their potential effects on physical work load," *Ergonomics*, vol. 59, no. 5, pp. 671–681, 2016.

[6] S. H. Collins, M. B. Wiggin, and G. S. Sawicki, "Reducing the energy cost of human walking using an unpowered exoskeleton," *Nature*, vol. 522, no. 7555, pp. 212–215, 2015.

[7] M. Windrich, M. Grimmer, O. Christ, S. Rinderknecht, and P. Beckerle, "Active lower limb prosthetics: A systematic review of design issues and solutions," *Biomed. Eng. Online*, vol. 15, no. 3, pp. 5–19, 2016.

[8] F. Heremans, S. Vijayakumar, M. Bouri, B. Dehez, and R. Ronsse, "Bio-inspired design and validation of the efficient lockable spring ankle (ELSA) prosthesis," in *Proc. IEEE 16th Int. Conf. Rehabil. Robot.*, 2019, pp. 411–416.

[9] L. M. Mooney, E. J. Rouse, and H. M. Herr, "Autonomous exoskeleton reduces metabolic cost of human walking during load carriage," *J. Neuroeng. Rehabil.*, vol. 11, no. 1, pp. 1–11, 2014.

[10] P. Malcolm, W. Derave, S. Galle, and D. De Clercq, "A simple exoskeleton that assists plantarflexion can reduce the metabolic cost of human walking," *PLoS One*, vol. 8, no. 2, 2013, Art. no. e 56137.

[11] K. Seo, J. Lee, Y. Lee, T. Ha, and Y. Shim, "Fully autonomous hip exoskeleton saves metabolic cost of walking," in *Proc. IEEE Int. Conf. Robot. Automat.*, 2016, pp. 4628–4635.

[12] F. A. Panizzolo *et al.*, "A biologically-inspired multi-joint soft exosuit that can reduce the energy cost of loaded walking," *J. Neuroeng. Rehabil.*, vol. 13, no. 1, pp. 1–14, 2016.

[13] A. B. Zoss, H. Kazerooni, and A. Chu, "Biomechanical design of the berkeley lower extremity exoskeleton (BLEEX)," *IEEE/ASME Trans. Mechatronics*, vol. 11, no. 2, pp. 128–138, Apr. 2006.

[14] E. Martini *et al.*, "Gait training using a robotic hip exoskeleton improves metabolic gait efficiency in the elderly," *Sci. Rep.*, vol. 9, no. 1, 2019, Art. no. 7157.

[15] R. Suzman and J. Beard, "Global health and aging," *NIH Publications*, vol. 1, no. 4, pp. 273–277, 2011.

[16] R. Suzman, J. R. Beard, T. Boerma, and S. Chatterji, "Health in an ageing world-what do we know?," *Lancet*, vol. 385, no. 9967, pp. 484–486, 2015.

[17] S. F. M. Chastin, E. Ferriolli, N. A. Stephens, K. C. Fearon, and C. Greig, "Relationship between sedentary behaviour, physical activity, muscle quality and body composition in healthy older adults," *Age Ageing*, vol. 41, no. 1, pp. 111–114, 2011.

[18] S. Galle, P. Malcolm, S. H. Collins, and D. De Clercq, "Reducing the metabolic cost of walking with an ankle exoskeleton: Interaction between actuation timing and power," *J. Neuroeng. Rehabil.*, vol. 14, no. 1, pp. 1–16, 2017.

[19] B. Quinlivan *et al.*, "Assistance magnitude versus metabolic cost reductions for a tethered multiarticular soft exosuit," *Sci. Robot.*, vol. 2, no. 2, 2017, Art. no. 4416.

[20] A. J. Young, J. Foss, H. Gannon, and D. P. Ferris, "Influence of power delivery timing on the energetics and biomechanics of humans wearing a hip exoskeleton," *Front. Bioeng. Biotechnol.*, vol. 5, pp. 1–11, 2017.

[21] Y. Ding *et al.*, "Effect of timing of hip extension assistance during loaded walking with a soft exosuit," *J. Neuroeng. Rehabil.*, vol. 13, no. 1, pp. 1–10, 2016.

[22] I. Kang, H. Hsu, and A. Young, "The effect of hip assistance levels on human energetic cost using robotic hip exoskeletons," *IEEE Robot. Automat. Lett.*, vol. 4, no. 2, pp. 430–437, Apr. 2019.

[23] D. Winter and H. Yack, "EMG profiles during normal human walking: Stride-to-stride and inter-subject variability," *Electroencephalogr. Clin. Neuriophysiol.*, vol. 67, no. 5, pp. 402–411, 1987.

[24] M. P. Murray, "Gait as a total pattern of movement: Including a bibliography on gait," *Amer. J. Phys. Med. Rehabil.*, vol. 46, no. 1, pp. 290–333, 1967.

[25] M. P. Murray, A. B. Drought, and R. C. Kory, "Walking patterns of normal men," *J. Bone Joint Surg.*, vol. 46, no. 2, pp. 335–360, 1964.

[26] J. R. Koller, D. H. Gates, D. P. Ferris, and C. D. Remy, "'Body-in-the-loop' optimization of assistive robotic devices: A validation study," *Robot., Sci. Syst.*, vol. 2016, pp. 1–10, 2016.

[27] J. Zhang *et al.*, "Human-in-the-loop optimization of exoskeleton assistance during walking," *Science*, vol. 356, no. 6344, pp. 1280–1284, 2017.

[28] Y. Ding, M. Kim, S. Kuindersma, and C. J. Walsh, "Human-in-the-loop optimization of hip assistance with a soft exosuit during walking," *Sci. Robot.*, vol. 3, no. 15, 2018, Art. no. eaar 5438.

[29] W. Felt, J. C. Selinger, J. M. Donelan, and C. D. Remy, "'Body-in-the-loop': Optimizing device parameters using measures of instantaneous energetic cost," *PLoS One*, vol. 10, no. 8, 2015, Art. no. e0 135342.

[30] M. Kim *et al.*, "Human-in-the-loop Bayesian optimization of wearable device parameters," *PLoS One*, vol. 12, no. 9, 2017, Art. no. e0 184054.

[31] D. F. N. Gordon, T. Matsubara, T. Noda, T. Teramae, J. Morimoto, and S. Vijayakumar, "Bayesian optimisation of exoskeleton design parameters," in *Proc. 7th IEEE Int. Conf. Biomed. Robot. Biomechatronics*, 2018, pp. 653–658.

[32] G. Lv, H. Xing, J. Lin, R. D. Gregg, and C. G. Atkeson, "A task-invariant learning framework of lower-limb exoskeletons for assisting human locomotion," in *Proc. Amer. Control Conf.*, 2020, pp. 569–576.

[33] M. Hamaya, T. Matsubara, T. Noda, T. Teramae, and J. Morimoto, "Learning assistive strategies for exoskeleton robots from user-robot physical interaction," *Pattern Recognit. Lett.*, vol. 99, pp. 67–76, 2017.

[34] M. Hamaya *et al.*, "Exploiting human and robot muscle synergies for human-in-the-loop optimization of EMG-based assistive strategies," in *Proc. Int. Conf. Robot. Automat.*, 2019, pp. 549–555.

[35] M. Tucker *et al.*, "Preference-based learning for exoskeleton gait optimization," in *Proc. IEEE Int. Conf. Robot. Automat.*, 2020, pp. 2351–2357.

[36] X. Tu, M. Li, M. Liu, J. Si, and H. H. Huang, "A data-driven reinforcement learning solution framework for optimal and adaptive personalization of a hip exoskeleton," in *Proc. IEEE Int. Conf. Robot. Automat.*, 2021, pp. 10 610–10616.

[37] Y. Wen, J. Si, A. Brandt, X. Gao, and H. H. Huang, "Online reinforcement learning control for the personalization of a robotic knee prosthesis," *IEEE Trans. Cybern.*, vol. 50, no. 6, pp. 2346–2356, Jun. 2020.

[38] M. Li, Y. Wen, X. Gao, J. Si, and H. Huang, "Toward expedited impedance tuning of a robotic prosthesis for personalized gait assistance by reinforcement learning control," *IEEE Trans. Robot.*, to be published, doi: 10.1109/TRO.2021.3078317.

[39] Y. Wen, M. Li, J. Si, and H. Huang, "Wearer-prosthesis interaction for symmetrical gait: A study enabled by reinforcement learning prosthesis control," *IEEE Trans. Neural Syst. Rehabil. Eng.*, vol. 28, no. 4, pp. 904–913, Apr. 2020.

[40] J. C. Selinger and J. M. Donelan, "Estimating instantaneous energetic cost during non-steady-state gait," *J. Appl. Physiol.*, vol. 117, no. 11, pp. 1406–1415, 2014.

[41] H. Westerblad, J. D. Bruton, and A. Katz, "Skeletal muscle: Energy metabolism, fiber types, fatigue and adaptability," *Exp. Cell Res.*, vol. 316, no. 18, pp. 3093–3099, 2010.

[42] M. Kim *et al.*, "Bayesian optimization of soft exosuits using a metabolic estimator stopping process," in *Proc. Int. Conf. Robot. Automat.*, 2019, pp. 9173–9179.

[43] P. Slade, R. Troutman, M. J. Kochenderfer, S. H. Collins, and S. L. Delp, "Rapid energy expenditure estimation for ankle assisted and inclined loaded walking," *J. Neuroeng. Rehabil.*, vol. 16, no. 1, pp. 1–10, 2019.

[44] S. L. Delp *et al.*, "Opensim: Open-source software to create and analyze dynamic simulations of movement," *IEEE Trans. Biomed. Eng.*, vol. 54, no. 11, pp. 1940–1950, Nov. 2007.

[45] G. Henderson, D. Gordon, and S. Vijayakumar, "Identifying invariant gait metrics for exoskeleton assistance," in *Proc. IEEE Int. Conf. Robot. Biomimetics*, 2017, pp. 520–526.

[46] D. F. Gordon, G. Henderson, and S. Vijayakumar, "Effectively quantifying the performance of lower-limb exoskeletons over a range of walking conditions," *Front. Robot. AI*, vol. 5, p. 61, 2018, doi: 10.3389/frobt.2018.00061.

[47] C. L. Dembia, A. Silder, T. K. Uchida, J. L. Hicks, and S. L. Delp, "Simulating ideal assistive devices to reduce the metabolic cost of walking with heavy loads," *PLoS One*, vol. 12, no. 7, 2017, Art. no. e0 180320.

[48] G. T. Yamaguchi and F. E. Zajac, "A planar model of the knee joint to characterize the knee extensor mechanism," *J. Biomech.*, vol. 22, no. 1, pp. 1–10, 1989.

[49] S. L. Delp, J. P. Loan, M. G. Hoy, F. E. Zajac, E. L. Topp, and J. M. Rosen, "An interactive graphics-based model of the lower extremity to study orthopaedic surgical procedures," *IEEE Trans. Biomed. Eng.*, vol. 37, no. 8, pp. 757–767, Aug. 1990.

[50] F. C. Anderson and M. G. Pandy, "A dynamic optimization solution for vertical jumping in three dimensions," *Comput. Methods Biomech. Biomed. Eng.*, vol. 2, no. 3, pp. 201–231, 1999.

[51] F. C. Anderson and M. G. Pandy, "Dynamic optimization of human walking," *J. Biomech. Eng.*, vol. 123, no. 5, pp. 381–390, 2001.

[52] B. R. Umberger, K. G. Gerritsen, and P. E. Martin, "A model of human muscle energy expenditure," *Comput. Methods Biomech. Biomed. Eng.*, vol. 6, no. 2, pp. 99–111, 2003.
[53] T. K. Uchida, J. L. Hicks, C. L. Dembia, and S. L. Delp, "Stretching your energetic budget: How tendon compliance affects the metabolic cost of running," *PLoS One*, vol. 11, no. 3, 2016, Art. no. e0 150378.
[54] T. K. Uchida, A. Seth, S. Pouya, C. L. Dembia, J. L. Hicks, and S. L. Delp, "Simulating ideal assistive devices to reduce the metabolic cost of running," *PLoS One*, vol. 11, no. 9, 2016, Art. no. e0 163417.
[55] A. D. Koelewijn, D. Heinrich, and A. J. Van Den Bogert, "Metabolic cost calculations of gait using musculoskeletal energy models, a comparison study," *PLoS One*, vol. 14, no. 9, 2019, Art. no. e0222037.
[56] F. Giovacchini *et al.*, "A light-weight active orthosis for hip movement assistance," *Robot. Auton. Syst.*, vol. 73, pp. 123–134, 2015.
[57] E. Martini, *et al.*, "Lower-limb amputees can reduce the energy cost of walking when assisted by an active pelvis orthosis," in *Proc. 8th IEEE RAS/EMBS Int. Conf. Biomed. Robot. Biomechatron.*, 2020, p. 809–815.
[58] R. Ronsse *et al.*, "Oscillator-based assistance of cyclical movements: Model-based and model-free approaches," *Med. Biol. Eng. Comput.*, vol. 49, no. 10, 2011, Art. no. 1173.
[59] D. A. Winter, "Biomechanical motor patterns in normal walking," *J. Motor Behav.*, vol. 15, no. 4, pp. 302–330, 1983.
[60] A. Seth *et al.*, "Opensim: Simulating musculoskeletal dynamics and neuromuscular control to study human and animal movement," *PLoS Comput. Biol.*, vol. 14, no. 7, 2018, Art. no. e 1006223.
[61] M. M. van der Krogt, L. Bar-On, T. Kindt, K. Desloovere, and J. Harlaar, "Neuro-musculoskeletal simulation of instrumented contracture and spasticity assessment in children with cerebral palsy," *J. Neuroeng. Rehabil.*, vol. 13, no. 1, pp. 1–11, 2016.
[62] M. S. DeMers, J. L. Hicks, and S. L. Delp, "Preparatory co-activation of the ankle muscles may prevent ankle inversion injuries," *J. Biomech.*, vol. 52, pp. 17–23, 2017.
[63] C. T. John, F. C. Anderson, J. S. Higginson, and S. L. Delp, "Stabilisation of walking by intrinsic muscle properties revealed in a three-dimensional muscle-driven simulation," *Comput. Methods Biomech. Biomed. Eng.*, vol. 16, no. 4, pp. 451–462, 2013.
[64] H. Kainz *et al.*, "Reliability of four models for clinical gait analysis," *Gait Posture*, vol. 54, pp. 325–331, 2017.
[65] "Gait 2392 and 2354 models," Accessed: Sep. 30, 2010. [Online]. Available: https://simtk-confluence.stanford.edu/display/OpenSim/Gait+2392+and+2354+Models
[66] M. A. Sherman, A. Seth, and S. L. Delp, "Simbody: Multibody dynamics for biomedical research," *Procedia Iutam*, vol. 2, pp. 241–261, 2011.
[67] D. G. Thelen, "Adjustment of muscle mechanics model parameters to simulate dynamic contractions in older adults," *J. Biomechanical Eng.*, vol. 125, no. 1, pp. 70–77, 2003.
[68] M. A. Sherman, A. Seth, and S. L. Delp, "What is a moment arm? calculating muscle effectiveness in biomechanical models using generalized coordinates," in *Proc. ASME Des. Eng. Tech. Conf.*, 2013, pp. 1–9.
[69] F. C. Anderson and M. G. Pandy, "Static and dynamic optimization solutions for gait are practically equivalent," *J. Biomech.*, vol. 34, no. 2, pp. 153–161, 2001.
[70] Y.-C. Lin, T. W. Dorn, A. G. Schache, and M. G. Pandy, "Comparison of different methods for estimating muscle forces in human movement," *Proc. Inst. Mech. Eng., Part H: J. Eng. Med.*, vol. 226, no. 2, pp. 103–112, Feb. 2012.
[71] J. Snoek, H. Larochelle, and R. P. Adams, "Practical Bayesian optimization of machine learning algorithms," in *Proc. Adv. Neural Inf. Process. Syst.*, 2012, pp. 2951–2959.
[72] C. L. Vaughan and M. J. O'Malley, "Froude and the contribution of naval architecture to our understanding of bipedal locomotion," *Gait Posture*, vol. 21, no. 3, pp. 350–362, 2005.
[73] O. S. Mian, J. M. Thom, L. P. Ardigó, M. V. Narici, and A. E. Minetti, "Metabolic cost, mechanical work, and efficiency during walking in young and older men," *Acta physiologica*, vol. 186, no. 2, pp. 127–139, 2006.
[74] J. Brockway, "Derivation of formulae used to calculate energy expenditure in man," *Human Nutr. Clin. Nutr.*, vol. 41, no. 6, pp. 463–471, 1987.
[75] M. M. Arones, M. S. Shourijeh, C. Patten, and B. J. Fregly, "Musculoskeletal model personalization affects metabolic cost estimates for walking," *Front. Bioeng. Biotechnol.*, vol. 8, pp. 1–12, 2020.
[76] G. Serrancolí, A. L. Kinney, and B. J. Fregly, "Influence of musculoskeletal model parameter values on prediction of accurate knee contact forces during walking," *Med. Eng. Phys.*, vol. 85, pp. 35–47, 2020.
[77] A. Muller, D. Haering, C. Pontonnier, and G. Dumont, "Non-invasive techniques for musculoskeletal model calibration," in *Proc. Congrès Fr. de Mécanique*, 2017, pp. 1–21.

Daniel F. N. Gordon received the M.Math. degree in mathematics from the University of St Andrews, St Andrews, Scotland, in 2014, the M.Sc.(R) degree in robotics and autonomous systems and the Ph.D. degree in exoskeleton-assisted locomotion from the University of Edinburgh, Edinburgh, Scotland, in 2016 and 2021, respectively.

Since 2019, he has been a Research Associate with the University of Edinburgh, exploring topics related to the control, design and evaluation of exoskeletons. His research interests include gait analysis, musculoskeletal modeling, optimization, and the control of assistive robotic devices including exoskeletons and prosthetic limbs.

Christopher McGreavy received the M.Sc. degree in computational neuroscience and cognitive robotics from the University of Birmingham, Birmingham, U.K., in 2016, and the M.Sc.(R) degree in 2018 in robotics and autonomous systems from the University of Edinburgh, Edinburgh, U.K., where he is currently working toward the Ph.D. degree in robotics and autonomous systems.

His research interests include robotic and human locomotion, enhancing understanding and application of dynamic, and efficient legged locomotion.

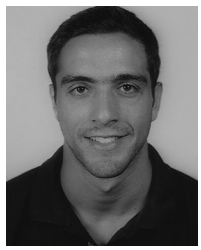

Andreas Christou received the M.Eng. degree in mechanical engineering in 2019 from the University of Edinburgh, Edinburgh, U.K., where he is currently working toward the Ph.D. degree in robotics and autonomous systems.

His research interests include robotic rehabilitation, wearable robots, human augmentation, and functional electrical stimulation.

Sethu Vijayakumar received the Ph.D. degree in computer science and engineering from the Tokyo Institute of Technology, Tokyo, Japan, in 1998.

He is the Professor of Robotics with the University of Edinburgh, an adjunct faculty of the University of Southern California, Los Angeles and the founding Director of the Edinburgh Centre for Robotics. His research interests include statistical machine learning, anthropomorphic robotics, planning, multiobjective optimization, and optimal control in autonomous systems as well as the study of human motor control.

Prof. Vijayakumar helps shape and drive the national Robotics and Autonomous Systems agenda in his recent role as the Programme Co-Director for artificial intelligence with the Alan Turing Institute, U.K.'s national institute for the Data Science and AI. He is a Fellow of the Royal Society of Edinburgh, a judge on BBC Robot Wars, and winner of the 2015 Tam Dalyell Prize for excellence in engaging the public with science.